First-principles density-functional calculations for optical spectra of clusters and nanocrystals

Igor Vasiliev,* Serdar Öğüt, and James R. Chelikowsky
Department of Chemical Engineering and Materials Science, Minnesota Supercomputing Institute, University of Minnesota, Minneapolis, Minnesota 55455

(Received 20 June 2001; revised manuscript received 1 October 2001; published 8 March 2002)

Electronic and structural calculations for atomic clusters present many challenges for traditional theoretical methods. While the computational framework for ground-state properties of clusters is relatively well established, calculations for excited states remain difficult. In this paper we implement a linear-response theory within the time-dependent local density approximation (TDLDA) and apply this technique to calculate excitation energies and optical absorption spectra for a variety of systems ranging from single atoms to semiconductor quantum dots up to several hundred atoms in size. The TDLDA formalism represents a fully *ab initio* formalism for excited states that avoids many of the drawbacks associated with empirical or semiempirical methods. Compared to other *ab initio* techniques for excited states, the TDLDA method requires considerably less computational effort and can be applied to much larger systems. We find the computed excitation energies, photoabsorption spectra, and optical absorption gaps to be in good agreement with available experimental data. Our calculations show that the accuracy of the TDLDA method in the range of lower transition energies is often comparable to that of more computationally intensive techniques, such as methods based on the exact exchange, optimized effective potential, or on solving the Bethe-Salpeter equation within the *GW* approximation.

DOI: 10.1103/PhysRevB.65.115416 PACS number(s): 73.22.−f, 71.15.Mb, 71.15.Qe, 71.35.Cc

I. INTRODUCTION

The influence of physical dimensions on the properties of materials becomes increasingly important as the size of semiconductor integrated circuits continues to shrink. The study of atomic clusters and nanocrystals provide a key to microscopic understanding of size-related effects. Electronic and structural calculations for clusters can help explain such phenomena as quantum confinement, surface reconstruction, and crystal growth, describe the formation of surface and bulk defects, and predict the properties of porous and disordered materials.

Because of a large number of atoms and the lack of general symmetry, computer simulations for clusters pose formidable challenges for traditional theoretical methods. Simple and cost-efficient ''classical'' methods based on empirical force fields or interatomic potentials often do not work well for clusters. The reconstruction of surfaces and the strong electronic delocalization make clusters difficult to describe through interatomic interactions derived from the crystalline state.[1] For this reason, accurate calculations for clusters usually require a direct quantum mechanical approach. Among such methods, *ab initio* pseudopotential techniques based on density-functional theory (DFT) within the local density approximation (LDA) attract special interest.[2]

The combination of the LDA and the pseudopotential approach has proved to be very successful for predicting the structural and cohesive properties of various solids.[3] The pseudopotential approximation removes the chemically inert core electrons from the problem, effectively reducing the number of particles in the quantum mechanical equations. In the absence of core states, pseudo-wave functions are smoothly varying and can be easily represented within any chosen basis. For localized systems such as clusters and molecules, a direct real-space implementation of this technique is particularly advantageous.[4] With this approach, the Schrödinger equation for electronic states is solved on a real-space three-dimensional grid within a spherical boundary domain, and the kinetic energy operator is approximated by a higher-order finite difference expansion on grid points.[5] Unlike ''supercell'' calculations in momentum space,[6] real-space methods do not produce an artificial periodicity, and do not impose restrictions on the net charge of the system.

One of the most significant limitations of conventional density functional formalism is its inability to deal with electronic excitations. Within time-independent density functional theory, the state of a quantum mechanical system is described through the ground-state electronic charge density. While this approach can be accurate for the ground state of a many-electron system, the excited electronic states are not adequately represented by the time-independent formalism.[7] The inability to describe excitations severely restricts the range of applications for conventional density functional methods, since many important physical properties such as optical absorption and emission, response to time-dependent fields, the dynamic dielectric function, and the band gap in semiconductors are associated with excited states.

Explicit calculations for excited states present enormous challenges for theoretical methods. Accurate calculations for excitation energies and absorption spectra typically require complex computational techniques, such as the configuration interaction method,[8] quantum Monte Carlo simulations,[9] or the Green's function method based on the GW approximation.[10] While these methods describe electronic excitations properly, they are usually limited to very small systems because of high computational demands. Alternatively, our calculations for excited-state properties employ a technique based on linear-response theory within the *time-*

dependent density-functional formalism and the local density approximation (TDLDA).[7,11,12] The TDLDA technique can be viewed as a natural extension of the ground-state density-functional LDA formalism, designed to include the proper representation of excited states. Within TDLDA, the true excitation energies of a many-electron system are computed from the conventional, time-independent Kohn-Sham transition energies and wave functions. Compared to other theoretical methods for excited states, the TDLDA technique requires considerably less computational effort and can be applied to much larger systems. Despite its relative simplicity, the TDLDA method incorporates screening and relevant correlation effects for electronic excitations.[7,11] In this sense, TDLDA represents a fully *ab initio* formalism for excited states.

We implemented the TDLDA technique entirely in real space within a higher-order finite-difference pseudopotential method.[4] The real-space implementation represents a natural choice for this technique due to the real-space formulation of TDLDA theory. With other methods, such as the plane-wave technique, TDLDA calculations usually require an intermediate real-space basis,[13] which complicates calculations and could introduce implementation errors. The direct real-space approach simplifies implementation and allows calculation of TDLDA optical response in a single step. We have applied this technique to compute transition energies and optical absorption spectra for many different systems ranging from single atoms to semiconductor quantum dots up to several hundred atoms in size.[12,14,15] In this paper, we provide a detailed description of the real-space TDLDA formalism and present an overview of our TDLDA calculations for various systems.

II. THEORETICAL METHODS

A. Finite difference pseudopotential method

Prior to computing excitation energies and absorption spectra, we solve the general electronic problem for the structure of interest. Our computational approach is based on a higher-order finite-difference pseudopotential method within density functional theory.[4] The electronic problem is defined by a set of the Kohn-Sham equations in the form

$$\left(-\frac{\nabla^2}{2}+\sum_a v_{\rm ion}(\mathbf{r}-\mathbf{R}_a)+v_{\rm H}[\rho](\mathbf{r})+v_{\rm xc}[\rho](\mathbf{r})\right)\psi_i(\mathbf{r}) = \epsilon_i\psi_i(\mathbf{r}). \quad (1)$$

Atomic units are used throughout unless otherwise specified. In Eq. (1), the true potential of each ion at $\mathbf{R}_a$ is replaced by a pseudopotential $v_{\rm ion}(\mathbf{r}-\mathbf{R}_a)$, which accounts for the interaction with core electrons and nuclei, the Hartree potential, $v_{\rm H}[\rho](\mathbf{r})$, describes the electrostatic interactions among valence electrons, and the exchange-correlation potential, $v_{\rm xc}[\rho](\mathbf{r})$, represents the nonclassical part of the Hamiltonian. $\rho(\mathbf{r})$ is the charge density. The single-electron Kohn-Sham eigenvalues ϵ_i and eigen-wave functions $\psi_i(\mathbf{r})$ pertain to valence electrons only.

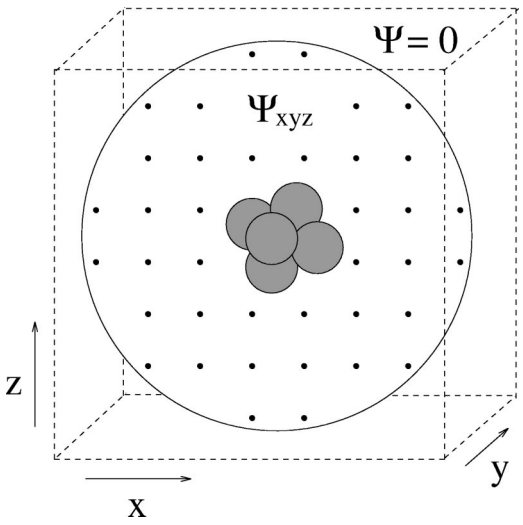

FIG. 1. Schematic illustration of the boundary domain for a cluster.

The potentials and electronic wave functions are set up on a simple Cartesian three-dimensional grid within a spherical domain, as shown schematically in Fig. 1. The grid points inside the sphere are described by their discrete space coordinates, $\{x,y,z\}$. Outside the boundary domain wave functions are required to vanish. The kinetic energy term $-\nabla^2/2$ is approximated by a higher-order finite-difference expansion for the Laplacian operator, which replaces spatial derivatives with a weighted sum of the wave-function values at neighboring grid points,

$$\nabla^2\psi_i(x,y,z)=\frac{1}{h^2}\sum_{n=-N}^{N} C_{N,n}^{\{2\}}[\psi_i(x+nh,y,z) + \psi_i(x,y+nh,z)+\psi_i(x,y,z+nh)]. \quad (2)$$

In this equation, h is the grid spacing and $C_{N,n}^{\{2\}}$ are the coefficients in the order-N finite-difference expansion for the second derivative. The numerical values of the expansion coefficients are readily available in literature.[16] For a given accuracy of calculations, the finite-difference order should be chosen as a compromise between having a fine grid and a large but sparse Hamiltonian matrix, versus having a coarse grid and a small but less sparse matrix. In electronic structure calculations, a finite difference expansion between the fourth and sixth orders typically presents the optimum choice.[4]

The nonlocal ionic pseudopotential simulates the angular-momentum-dependent interaction between the valence and core electrons. We employ the Kleinman-Bylander[17] form of the nonlocal pseudopotential,

$$v_{\rm ion}(\mathbf{r}-\mathbf{R}_a)\psi_i(\mathbf{r})=v_{\rm local}(\mathbf{r}-\mathbf{R}_a)\psi_i(\mathbf{r}) + \sum_{l,m} G_{lm}\Delta v_l(\mathbf{r}-\mathbf{R}_a)\phi_{lm}(\mathbf{r}-\mathbf{R}_a), \quad (3)$$

where $v_{\rm local}$ is the local ionic pseudopotential, $\Delta v_l = v_l - v_{\rm local}$ is the difference between the local potential and the

potential component with the angular momentum l, ϕ_{lm} are the atomic pseudo-wave functions, and the projection coefficients G_{lm} are calculated as

$$G_{lm}=\frac{\langle \phi_{lm}|\Delta v_l|\psi_i\rangle}{\langle \phi_{lm}|\Delta v_l|\phi_{lm}\rangle}. \tag{4}$$

In real space, the Kleinman-Bylander form of the pseudopotential limits the nonlocality to a small region around each atom. All calculations presented in this article employed Troullier-Martins pseudopotentials.[18]

The exchange-correlation potential within LDA is approximated by a functional of the charge density. In our calculations, we used a parametrized form of the Ceperley-Alder functional.[19] The parametrization formula and its coefficients will be further discussed in later sections. Owing to the nonlinear nature of the LDA exchange-correlation functional, the accuracy of the approximation can be improved by correcting the formula to account for the core charge density. The exchange-correlation potential is then evaluated as a functional of the *core-corrected* charge density,

$$\rho(\mathbf{r})=\rho_v(\mathbf{r})+\sum_a \rho_{\rm core}(|\mathbf{r}-\mathbf{R}_a|), \tag{5}$$

where $\rho_{\rm core}(|\mathbf{r}-\mathbf{R}_a|)$ is a fixed partial correction for the core charge density[20] and $\rho_v(\mathbf{r})$ is the *valence* charge density calculated as

$$\rho_v(\mathbf{r})=\sum_i n_i|\psi_i(\mathbf{r})|^2, \tag{6}$$

where $\psi_i(\mathbf{r})$ are single-electron wave functions and n_i are occupation numbers.

Within this recipe, the off-diagonal elements of the Hamiltonian matrix are produced only by the kinetic energy and the nonlocal part of the ionic pseudopotential. All other terms, including the local part of the pseudopotential, the Hartree potential, and the exchange-correlation potential, contribute only to the main diagonal of the Hamiltonian. The Hartree potential is obtained by setting up and solving the Poisson equation for the charge density by the conjugate-gradient method,[21]

$$\nabla^2 v_{\rm H}[\rho](\mathbf{r})=-4\pi\rho_v(\mathbf{r}). \tag{7}$$

To solve the Poisson equation numerically, we use a higher-order finite difference expansion for the Laplacian operator, similar to one given by Eq. (2). The boundary conditions for the Poisson equation on points outside of the main domain are determined by a multipole expansion of the charge density. For large systems, the Poisson equation method is significantly more efficient than the direct summation over the grid points.

After the Hamiltonian matrix is set up, the system of Kohn-Sham equations for electronic states must be solved self-consistently. The initial charge-density distribution is constructed by superposing atomic charge densities. Based on the initial charge density, we calculate the Hartree and exchange-correlation potentials, and set up the Hamiltonian matrix. The matrix equation is solved numerically by iterative diagonalization using the generalized Davidson algorithm.[21,22] From the solution of this matrix equation we obtain a new distribution of the charge density. The self-consistent procedure is repeated until we achieve the desired convergence of the numerical solution. The convergence criterion in our calculations is defined by the root-mean-square difference between the input and output potentials. Typically, we require this difference to be less than 10^{-4} a.u.

B. Time-dependent density-functional theory

The central theorem of density-functional theory states that the external potential and the ground-state energy of a system of interacting electrons are uniquely determined by the ground-state charge density.[2] However, the classic formulation of the density-functional formalism is restricted to the *time-independent* case only. A proper treatment of electronic excitations is not possible within the time-independent framework and requires a generalization of DFT to the time-dependent phenomena. This limitation has led to the development of *time-dependent* density functional theory (TDDFT).[23,24] Within TDDFT, the main theorem of the density-functional formalism is extended to time-dependent systems. Similarly, to the case of time-independent DFT, the time-dependent formalism reduces the many-electron problem to a set of self-consistent single particle equations,[24]

$$\left(-\frac{\nabla^2}{2}+v_{\rm eff}[\rho](\mathbf{r},t)\right)\psi_i(\mathbf{r},t)=i\frac{\partial}{\partial t}\psi_i(\mathbf{r},t). \tag{8}$$

In this case, the single-particle wave functions $\psi_i(\mathbf{r},t)$ and the effective potential $v_{\rm eff}[\rho](\mathbf{r},t)$ explicitly depend on time. The effective potential is given by

$$v_{\rm eff}[\rho](\mathbf{r},t)=\sum_a v_{\rm ion}(\mathbf{r}-\mathbf{R}_a)+\int\frac{\rho_v(\mathbf{r}',t)}{|\mathbf{r}-\mathbf{r}'|}d\mathbf{r}' +v_{\rm xc}[\rho](\mathbf{r},t). \tag{9}$$

The three terms on the right-hand side of Eq. (9) describe the external ionic potential, the potential Hartree, and the exchange-correlation potential, respectively. In the adiabatic approximation, which is local in *time*, the exchange-correlation potential and its first derivative can be expressed in terms of the *time-independent* exchange-correlation energy $E_{\rm xc}[\rho]$,

$$v_{\rm xc}[\rho](\mathbf{r},t)\cong\frac{\delta E_{\rm xc}[\rho]}{\delta\rho(\mathbf{r})},$$

$$\frac{\delta v_{\rm xc}[\rho](\mathbf{r},t)}{\delta\rho(\mathbf{r}',t')}\cong\delta(t-t')\frac{\delta^2 E_{\rm xc}[\rho]}{\delta\rho(\mathbf{r})\,\delta\rho(\mathbf{r}')}. \tag{10}$$

The energy $E_{\rm xc}[\rho]$ in Eq. (10) can be further approximated by a regular LDA exchange-correlation functional,

$$E_{\rm xc}[\rho]=\int\rho(\mathbf{r})\epsilon_{\rm xc}(\rho(\mathbf{r}))d\mathbf{r}, \tag{11}$$

which is local in *space*.

C. Linear response in TDDFT

The linear-response formalism within TDDFT provides a theoretical basis for the TDLDA method. In this section, we illustrate how TDLDA excitation energies and oscillator strengths are derived from single-electron Kohn-Sham eigenvalues and eigen-wave functions. A comprehensive analysis of time-dependent density-functional response theory can be found elsewhere.[7,11] We use the general notation adapted from the work of Casida.[11]

The response of the Kohn-Sham density matrix within TDDFT is obtained by introducing a time-dependent perturbation $\delta v_{\rm appl}(\mathbf{r},t)$. Due to the self-consistent nature of the Kohn-Sham Hamiltonian, the *effective* perturbation includes the response of the self-consistent field $\delta v_{\rm SCF}[\rho](\mathbf{r},t)$,

$$\delta v_{\rm eff}[\rho](\mathbf{r},t)=\delta v_{\rm appl}(\mathbf{r},t)+\delta v_{\rm SCF}[\rho](\mathbf{r},t), \tag{12}$$

where the self-consistent field is given by the last two terms in Eq. (9),

$$v_{\rm SCF}[\rho](\mathbf{r},t)=\int \frac{\rho_v(\mathbf{r}',t)}{|\mathbf{r}-\mathbf{r}'|}d\mathbf{r}'+v_{\rm xc}[\rho](\mathbf{r},t). \tag{13}$$

In frequency space, the response of the Kohn-Sham density matrix $\delta\mathbf{P}(\omega)$ can be derived using the generalized susceptibility $\chi(\omega)$. For quasiindependent Kohn-Sham particles, the sum-over-states representation of the generalized susceptibility is given by

$$\chi_{ij\sigma,kl\tau}(\omega)=\delta_{i,k}\delta_{j,l}\delta_{\sigma,\tau}\frac{\lambda_{lk\tau}}{\omega-\omega_{lk\tau}}, \tag{14}$$

where $\lambda_{lk\tau}=n_{l\tau}-n_{k\tau}$ is the difference between the occupation numbers, and $\omega_{lk\tau}=\epsilon_{k\tau}-\epsilon_{l\tau}$ is the difference between the eigenvalues of the lth and kth single-particle states. The susceptibility in Eq. (14) is expressed in the basis of the unperturbed Kohn-Sham orbitals $\{\psi_{i\sigma}\}$ and the indices i, j, and σ (k, l, and τ) refer to space and spin wave components, respectively. The linear response of the density matrix is

$$\begin{aligned}\delta P_{ij\sigma}(\omega)&=\sum_{kl\tau}\chi_{ij\sigma,kl\tau}(\omega)\,\delta v^{\rm eff}_{kl\tau}(\omega)\\&=\frac{\lambda_{ji\sigma}}{\omega-\omega_{ji\sigma}}[\,\delta v^{\rm appl}_{ij\sigma}(\omega)+\delta v^{\rm SCF}_{ij\sigma}(\omega)].\end{aligned} \tag{15}$$

Equation (15) is, however, complicated by the fact that $\delta v_{\rm SCF}(\omega)$ depends on the response of the density matrix,

$$\delta v^{\rm SCF}_{ij\sigma}(\omega)=\sum_{kl\tau}K_{ij\sigma,kl\tau}\delta P_{kl\tau}(\omega), \tag{16}$$

where the coupling matrix $\mathbf{K}$ describes the response of the self-consistent field to changes in the charge density. Within the adiabatic approximation, this matrix is frequency-independent. The analytical expression for the adiabatic coupling matrix, $K_{ij\sigma,kl\tau}=\partial v^{\rm SCF}_{ij\sigma}/\partial P_{kl\tau}$, can be derived from Eq. (13) by making use of the functional chain rule,

$$\begin{aligned}K_{ij\sigma,kl\tau}=\int\int\psi^*_{i\sigma}(\mathbf{r})\psi_{j\sigma}(\mathbf{r})\Bigg(&\frac{1}{|\mathbf{r}-\mathbf{r}'|}\\&+\frac{\delta^2E_{\rm xc}[\rho]}{\delta\rho_\sigma(\mathbf{r})\,\delta\rho_\tau(\mathbf{r}')}\Bigg)\psi_{k\tau}(\mathbf{r}')\psi^*_{l\tau}(\mathbf{r}')d\mathbf{r}d\mathbf{r}'.\end{aligned} \tag{17}$$

The functional derivative in Eq. (17) is evaluated with respect to the *unperturbed* charge densities. By using the coupling matrix, Eq. (15) can be rewritten as

$$\begin{aligned}\sum_{kl\tau}^{\lambda_{kl\tau}\neq0}&\left[\delta_{i,k}\delta_{j,l}\delta_{\sigma,\tau}\frac{\omega-\omega_{lk\tau}}{\lambda_{lk\tau}}-K_{ij\sigma,kl\tau}\right]\delta P_{kl\tau}(\omega)\\&=\delta v^{\rm appl}_{ij\sigma}(\omega).\end{aligned} \tag{18}$$

Since the summation in Eq. (18) is performed over all occupied and unoccupied orbitals, it contains both the particle-hole and hole-particle contributions. These contributions can be written as two separate equations: the particle-hole part of $v_{\rm appl}(\omega)$ is given by

$$\begin{aligned}\sum_{kl\tau}^{\lambda_{kl\tau}>0}&\left[\delta_{i,k}\delta_{j,l}\delta_{\sigma,\tau}\frac{\omega-\omega_{lk\tau}}{\lambda_{lk\tau}}-K_{ij\sigma,kl\tau}\right]\delta P_{kl\tau}(\omega)\\&-\sum_{kl\tau}^{\lambda_{kl\tau}>0}K_{ij\sigma,lk\tau}\delta P_{lk\tau}(\omega)=\delta v^{\rm appl}_{ij\sigma}(\omega)\end{aligned} \tag{19}$$

and the hole-particle part of $v_{\rm appl}(\omega)$ is

$$\begin{aligned}\sum_{kl\tau}^{\lambda_{kl\tau}>0}&\left[\delta_{i,k}\delta_{j,l}\delta_{\sigma,\tau}\frac{\omega-\omega_{kl\tau}}{\lambda_{kl\tau}}-K_{ji\sigma,lk\tau}\right]\delta P_{lk\tau}(\omega)\\&-\sum_{kl\tau}^{\lambda_{kl\tau}>0}K_{ji\sigma,kl\tau}\delta P_{kl\tau}(\omega)=\delta v^{\rm appl}_{ji\sigma}(\omega).\end{aligned} \tag{20}$$

Combining Eqs. (19) and (20), one can separate the real and imaginary parts of the density-matrix response $\delta\mathbf{P}(\omega)$. If the basis functions $\{\psi_{i\sigma}\}$ in Eq. (17) are real, the coupling matrix $\mathbf{K}$ is also real and symmetric with respect to the interchange of space indices $i\leftrightarrow j$ and $k\leftrightarrow l$. Since $\delta\mathbf{P}(\omega)$ is Hermitian (i.e., $\delta P_{ji\sigma}=\delta P^*_{ij\sigma}$), the real part of $\delta\mathbf{P}(\omega)$ for a real perturbation $v_{\rm appl}(\omega)$ is given by

$$\begin{aligned}\sum_{kl\tau}^{\lambda_{kl\tau}>0}&\left[\frac{\delta_{i,k}\delta_{j,l}\delta_{\sigma,\tau}}{\lambda_{kl\tau}\omega_{kl\tau}}(\omega^2-\omega^2_{kl\tau})-2K_{ij\sigma,kl\tau}\right]{\rm Re}(\delta P_{kl\tau})(\omega)\\&=\delta v^{\rm appl}_{ij\sigma}(\omega),\end{aligned} \tag{21}$$

where ${\rm Re}(\delta P_{ij\sigma})(\omega)$ denotes the Fourier transform of the *real* part of $\delta P_{ij\sigma}(t)$.

Equation (21) can be used to obtain the density-functional expression for the dynamic polarizability. This is accomplished by introducing a perturbation $\delta\hat{v}_{\rm appl}(t)=\hat{\gamma}\mathcal{E}_\gamma(t)$, where $\mathcal{E}_\gamma$ is an external electric field applied along the γ axis, $\gamma=\{x,y,z\}$. The linear response of the dipole moment, $\delta\boldsymbol{\mu}(\omega)$, is expressed through of the real part of $\delta\mathbf{P}(\omega)$ as

$$\delta\mu_\beta(\omega) = -2 \sum_{ij\sigma}^{\lambda_{ij\sigma}>0} \beta_{ji\sigma} \mathrm{Re}(\delta P_{ij\sigma})(\omega), \quad \beta=\{x,y,z\}. \tag{22}$$

The components of the dynamic polarizability tensor are given by

$$\alpha_{\beta\gamma}(\omega) = \frac{\delta\mu_\beta(\omega)}{\mathcal{E}_\gamma(\omega)} = -\frac{2}{\mathcal{E}_\gamma(\omega)} \sum_{ij\sigma}^{\lambda_{ij\sigma}>0} \beta_{ji\sigma} \mathrm{Re}(\delta P_{ij\sigma})(\omega),$$

$$\beta,\gamma=\{x,y,z\}. \tag{23}$$

Solving Eq. (21) with respect to $\mathrm{Re}(\delta P_{ij\sigma})(\omega)$ and substituting the result into Eq. (23), one obtains the following matrix equation for the polarizability components:

$$\alpha_{\beta\gamma}(\omega) = 2\hat{\beta}\mathbf{R}^{1/2}[\mathbf{Q}-\omega^2\mathbf{1}]^{-1}\mathbf{R}^{1/2}\hat{\gamma}, \quad \beta,\gamma=\{x,y,z\}, \tag{24}$$

where the matrices $\mathbf{R}$ and $\mathbf{Q}$ are given by

$$R_{ij\sigma,kl\tau} = \delta_{i,k}\delta_{j,l}\delta_{\sigma,\tau}\lambda_{kl\tau}\omega_{kl\tau}, \tag{25}$$

$$Q_{ij\sigma,kl\tau} = \delta_{i,k}\delta_{j,l}\delta_{\sigma,\tau}\omega_{kl\tau}^2 + 2\sqrt{\lambda_{ij\sigma}\omega_{ij\sigma}}K_{ij\sigma,kl\tau}\sqrt{\lambda_{kl\tau}\omega_{kl\tau}}. \tag{26}$$

The TDLDA expressions for excitation energies and oscillator strengths can be derived by comparing Eq. (24) with the general sum-over-states formula for the average dynamic polarizability, $\langle\alpha(\omega)\rangle = \mathrm{tr}(\alpha_{\beta\gamma}(\omega))/3 = \Sigma_I f_I/(\Omega_I^2-\omega^2)$. The true excitation energies Ω_I, which correspond to the *poles* of the dynamic polarizability, are obtained from the solution of the eigenvalue problem,

$$\mathbf{Q}\mathbf{F}_I = \Omega_I^2\mathbf{F}_I. \tag{27}$$

The oscillator strengths f_I, which correspond to the *residues* of the dynamic polarizability, are given by

$$f_I = \frac{2}{3}\sum_{\beta=\{x,y,z\}} |\hat{\beta}\mathbf{R}^{1/2}\mathbf{F}_I|^2, \tag{28}$$

where $\mathbf{F}_I$ are the eigenvectors of Eq. (27).

D. Real-space implementation

The adiabatic TDLDA calculations for optical spectra require only the knowledge of the time-independent single-electron Kohn-Sham transition energies and wave functions. The most computationally demanding part in such calculations is the evaluation of the coupling matrix given by Eq. (17). This equation can be split into two parts: $\mathbf{K}=\mathbf{K}^{(I)}+\mathbf{K}^{(II)}$. The first term represents a double integral over $1/|\mathbf{r}-\mathbf{r}'|$. Instead of performing the costly double integration by direct summation, we calculate this term by solving the Poisson equation within the boundary domain. We employ the conjugate-gradient method to solve

$$\nabla^2\Phi_{ij\sigma}(\mathbf{r}) = -4\pi\psi_{i\sigma}(\mathbf{r})\psi_{j\sigma}(\mathbf{r}). \tag{29}$$

The first term in Eq. (17) is calculated as

$$K^{(I)}_{ij\sigma,kl\tau} = \int \Phi_{ij\sigma}(\mathbf{r})\psi_{k\tau}(\mathbf{r})\psi_{l\tau}(\mathbf{r})d\mathbf{r}. \tag{30}$$

The Poisson equation method provides a considerable speed-up as compared to the direct summation. The second term in Eq. (17) represents a double integral over the functional derivative of the exchange-correlation energy, $\delta^2E_{xc}[\rho]/\delta\rho_\sigma(\mathbf{r})\delta\rho_\tau(\mathbf{r}')$. Within the *local* approximation of the exchange-correlation potential this term is reduced to a single integral,

$$K^{(II)}_{ij\sigma,kl\tau} = \int \psi_{i\sigma}(\mathbf{r})\psi_{j\sigma}(\mathbf{r})\frac{\delta^2E_{xc}[\rho]}{\delta\rho_\sigma(\mathbf{r})\delta\rho_\tau(\mathbf{r})}\psi_{k\tau}(\mathbf{r})\psi_{l\tau}(\mathbf{r})d\mathbf{r}, \tag{31}$$

where the LDA exchange-correlation energy $E_{xc}[\rho]$ is given by Eq. (11).

Equation (31) requires the evaluation of the second derivatives for the LDA exchange-correlation energy with respect to spin-up and spin-down charge densities. The LDA *exchange* energy per particle is normally approximated by that of the homogeneous electron gas,[25]

$$\epsilon_x(\rho_\sigma(\mathbf{r})) = -\frac{3}{4\pi}[6\pi^2\rho_\sigma(\mathbf{r})]^{1/3}, \quad \sigma=\{\uparrow,\downarrow\}. \tag{32}$$

The first derivative of the total exchange energy determines the LDA exchange potential,

$$\frac{\delta E_x[\rho]}{\delta\rho_\sigma} = v_x[\rho_\sigma] = -\frac{1}{\pi}(6\pi^2\rho_\sigma)^{1/3}, \quad \sigma=\{\uparrow,\downarrow\}. \tag{33}$$

The second derivatives are

$$\frac{\delta^2E_x[\rho]}{\delta\rho_\uparrow\delta\rho_\uparrow} = -\left(\frac{2}{9\pi}\right)^{1/3}\rho_\uparrow^{-2/3}, \quad \frac{\delta^2E_x[\rho]}{\delta\rho_\uparrow\delta\rho_\downarrow} = 0. \tag{34}$$

We employ the Ceperley-Alder functional[19] for the LDA *correlation* energy. The Perdew-Zunger parametrization[26] of this functional is based on two different analytical expressions for $r_s<1$ and $r_s\geqslant 1$, where $r_s=(3/4\pi\rho)^{1/3}$ is the local Seitz radius and $\rho=\rho_\uparrow+\rho_\downarrow$. We slightly adjust the parametrization for $r_s<1$ to guarantee a continuous second derivative of the correlation energy. The adjusted interpolation formula for the correlation energy per particle is given by[27]

$$\epsilon_c^{U,P} = \begin{cases} A\ln r_s + B + Cr_s\ln r_s + Dr_s + Xr_s^2\ln r_s, & r_s<1 \\ \gamma/(1+\beta_1\sqrt{r_s}+\beta_2 r_s), & r_s\geqslant 1, \end{cases} \tag{35}$$

where two separate sets of coefficients are used for the *polarized spin* (P) and *unpolarized spin* (U) cases. The numerical values of all fitting parameters appearing in Eq. (35) are listed in Table I. Based on this interpolation formula, the first and second derivatives of the total correlation energy can be calculated as

TABLE I. Fitting parameters in the interpolation formula for the correlation energy given by Eq. (35). The majority of the interpolation coefficients, with the exception of C and X, coincide with the values suggested by Perdew and Zunger.[26] All values are in atomic units.

Spin	A	B	C	D	X	γ	β_1	β_2
Unpolarized	0.0311	−0.048	−0.0015	−0.0116	0.0036	−0.1423	1.0529	0.3334
Polarized	0.01555	−0.0269	−0.0005	−0.0048	0.0012	−0.0843	1.3981	0.2611

$$\frac{\delta E_c^{U,P}}{\delta\rho}=\frac{1}{3}[3A\ln r_s+3B-A+2Cr_s\ln r_s+(2D-C)r_s+Xr_s^2(\ln r_s-1)], \tag{36}$$

$$\frac{\delta^2 E_c^{U,P}}{\delta\rho^2}=-\frac{1}{9\rho}[3A+(2D+C)r_s+2Cr_s\ln r_s+Xr_s^2(2\ln r_s-1)], \tag{37}$$

for $r_s<1$ and

$$\frac{\delta E_c^{U,P}}{\delta\rho}=\frac{\gamma(6+7\beta_1\sqrt{r_s}+8\beta_2 r_s)}{6(1+\beta_1\sqrt{r_s}+\beta_2 r_s)^2}, \tag{38}$$

$$\frac{\delta^2 E_c^{U,P}}{\delta\rho^2}=\frac{\gamma[5\beta_1\sqrt{r_s}+(7\beta_1^2+8\beta_2)r_s+21\beta_1\beta_2 r_s^{3/2}+16\beta_2^2 r_s^2]}{36\rho(1+\beta_1\sqrt{r_s}+\beta_2 r_s)^3}, \tag{39}$$

for $r_s\geqslant 1$. The behavior of $\delta^2 E_c^{U,P}/\delta\rho^2$ in the vicinity of $r_s=1$ is shown in Fig. 2. The plot demonstrates that the adjusted interpolation formula for the correlation energy is indeed continuous up to its second derivative, while the original Perdew-Zunger parametrization is not.[26]

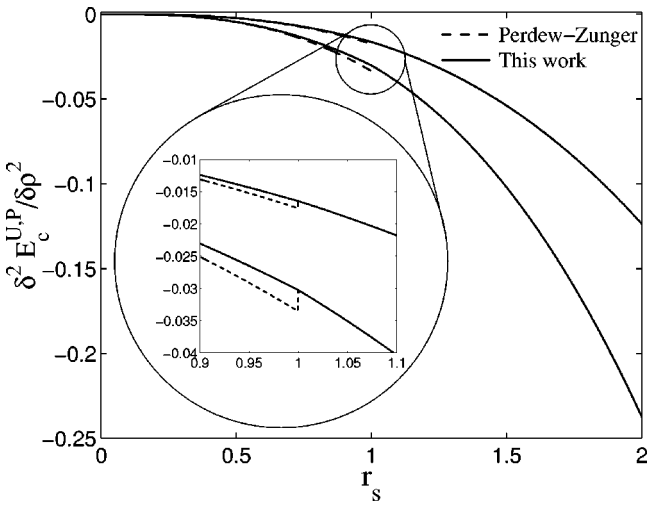

FIG. 2. Second derivative of the electronic correlation energy in the vicinity of $r_s=1$. For $r_s<1$, our parametrization slightly differ from that of Perdew and Zunger.[26] Both parametrizations coincide for $r_s\geqslant 1$.

Equations (35)–(39) describe only the cases of the completely polarized and unpolarized spin. For intermediate spin polarizations, the correlation energy can be obtained with a simple interpolation formula,

$$\epsilon_c=\epsilon_c^U+\xi(\rho)[\epsilon_c^P-\epsilon_c^U], \tag{40}$$

where

$$\xi(\rho)=\frac{1}{1-2^{-1/3}}(x_\uparrow^{4/3}+x_\downarrow^{4/3}-2^{-1/3});\quad x_\uparrow=\frac{\rho_\uparrow}{\rho},\quad x_\downarrow=\frac{\rho_\downarrow}{\rho}. \tag{41}$$

The expression for the second derivative of the correlation energy in case of an arbitrary spin polarization can be written as

$$\frac{\delta^2 E_c[\rho]}{\delta\rho_\sigma\delta\rho_\tau}=\frac{\delta^2 E_c^U}{\delta\rho^2}+\xi(\rho)\left(\frac{\delta^2 E_c^P}{\delta\rho^2}-\frac{\delta^2 E_c^U}{\delta\rho^2}\right)+\left(\frac{\partial\xi(\rho)}{\partial\rho_\sigma}+\frac{\partial\xi(\rho)}{\partial\rho_\tau}\right)\left(\frac{\delta E_c^P}{\delta\rho}-\frac{\delta E_c^U}{\delta\rho}\right)+\frac{\partial^2\xi(\rho)}{\partial\rho_\sigma\partial\rho_\tau}\times\rho(\epsilon_c^P-\epsilon_c^U),\quad \sigma,\tau=\{\uparrow,\downarrow\}, \tag{42}$$

where the spin polarization function $\xi(\rho)$ and its derivatives are given by

$$\frac{\partial\xi(\rho)}{\partial\rho_\uparrow}=\frac{4}{3\rho(1-2^{-1/3})}(x_\uparrow^{1/3}-x_\uparrow^{4/3}-x_\downarrow^{4/3}), \tag{43}$$

$$\frac{\partial^2\xi(\rho)}{\partial\rho_\uparrow\partial\rho_\uparrow}=\frac{4}{9\rho^2(1-2^{-1/3})}[x_\uparrow^{-2/3}-8x_\uparrow^{1/3}+7(x_\uparrow^{4/3}+x_\downarrow^{4/3})], \tag{44}$$

$$\frac{\partial^2\xi(\rho)}{\partial\rho_\uparrow\partial\rho_\downarrow}=\frac{4}{9\rho^2(1-2^{-1/3})}[7(x_\uparrow^{4/3}+x_\downarrow^{4/3})-4(x_\uparrow^{1/3}+x_\downarrow^{1/3})]. \tag{45}$$

E. Systems with unpolarized spin

The TDLDA formalism presented in previous sections can be further simplified for systems with the unpolarized spin. In this case, the spin-up and spin-down charge densities are equal, $\rho_\uparrow=\rho_\downarrow$, and Eqs. (41), (43)–(45) yield

$$\xi(\rho)=0, \quad \frac{\partial^2\xi(\rho)}{\partial\rho_\uparrow\partial\rho_\uparrow}=\frac{4}{9\rho^2(2^{1/3}-1)},$$

$$\frac{\partial\xi(\rho)}{\partial\rho_\uparrow}=0, \quad \frac{\partial^2\xi(\rho)}{\partial\rho_\uparrow\partial\rho_\downarrow}=-\frac{4}{9\rho^2(2^{1/3}-1)}. \tag{46}$$

Since the coordinate parts of spin-up and spin-down Kohn-Sham wave functions for systems with the unpolarized spin are identical, $\psi_{i\uparrow}=\psi_{i\downarrow}$, it follows that $Q_{ij\uparrow,kl\uparrow}=Q_{ij\downarrow,kl\downarrow}$ and $Q_{ij\uparrow,kl\downarrow}=Q_{ij\downarrow,kl\uparrow}$. This allows us to separate ''singlet'' and ''triplet'' transitions by representing Eq. (27) in the basis set of $\{\mathbf{F}_+,\mathbf{F}_-\}$, chosen as

$$F_{ij}^{\{+,-\}}=\frac{1}{\sqrt{2}}(F_{ij\uparrow}\pm F_{ij\downarrow}). \tag{47}$$

In this basis, the matrix $\mathbf{Q}$ becomes

$$Q_{ij,kl}^{\{+,-\}}=\delta_{i,k}\delta_{j,l}\omega_{kl}^2+2\sqrt{\lambda_{ij}\omega_{ij}}K_{ij,kl}^{\{+,-\}}\sqrt{\lambda_{kl}\omega_{kl}}, \tag{48}$$

where $K_{ij,kl}^{\{+,-\}}=K_{ij\uparrow,kl\uparrow}\pm K_{ij\uparrow,kl\downarrow}$. The components of $\mathbf{K}^{\{+,-\}}$ in their explicit form are given by

$$K_{ij,kl}^{+}=2\int\int\frac{\psi_i(\mathbf{r})\psi_j(\mathbf{r})\psi_k(\mathbf{r}')\psi_l(\mathbf{r}')}{|\mathbf{r}-\mathbf{r}'|}d\mathbf{r}d\mathbf{r}'$$
$$+2\int\psi_i(\mathbf{r})\psi_j(\mathbf{r})\left(\frac{\delta^2E_c^U}{\delta\rho^2}\right.$$
$$\left.-\frac{1}{(9\pi)^{1/3}\rho^{2/3}}\right)\psi_k(\mathbf{r})\psi_l(\mathbf{r})d\mathbf{r}, \tag{49}$$

$$K_{ij,kl}^{-}=2\int\psi_i(\mathbf{r})\psi_j(\mathbf{r})\left(\frac{4(\epsilon_c^P-\epsilon_c^U)}{9(2^{1/3}-1)}\right.$$
$$\left.-\frac{1}{(9\pi)^{1/3}\rho^{2/3}}\right)\psi_k(\mathbf{r})\psi_l(\mathbf{r})d\mathbf{r}. \tag{50}$$

For most practical applications, only ''singlet'' transitions represented by the $\mathbf{F}_+$ basis vectors are of interest. Triplet transitions described by the $\mathbf{F}_-$ vectors have zero dipole oscillator strength and do not contribute to optical absorption. By solving Eq. (27) for the $\mathbf{F}_+$ vectors only, we reduce the dimension of the eigenvalue problem by a factor of 2. Equations (48)–(50), however, can only be applied to systems with the unpolarized spin. In case of an arbitrary spin polarization, the general form of the matrix $\mathbf{Q}$ presented by Eq. (26) with the coupling matrix given by Eq. (17) and the functional derivatives given by Eqs. (33) through (45) must be used.

The coupling matrix $\mathbf{K}$ in general case includes transitions to both bound and unbound (continuum) electronic levels. While the eigenvalues and wave functions of bound states are relatively basis independent, the levels representing continuum strongly depend on the selected basis and boundary conditions imposed on the system. Unlike computational methods based on localized Gaussian-type orbitals,[28] calculations on a real-space grid do not require a special extension of the basis set to describe continuum states. Instead, the continuum is approximated by a finite number of unbound levels with *positive* Kohn-Sham eigenvalues localized inside the boundary domain. The accuracy of this approximation depends only on the size of the boundary domain and the number of unbound levels included in calculations. As such, it is always important to check for convergence of the TDLDA transition energies and oscillator strengths with respect to the size of the boundary domain and the number of unoccupied states included in the calculation of the coupling matrix.

So far, other than the adiabatic local density approximation, no other approximations have been made. The exact solution of the matrix equation (27) incorporates all relevant correlations among single-particle transitions. Assuming, for simplicity, the unpolarized spin case, we can derive approximate expressions for the TDLDA excitation energies. Let us assume that the coupling between different one-electron transitions is weak. Under this assumption we can neglect all matrix elements with $i\neq k$ and $j\neq l$. As a result, the coupling matrix becomes diagonal in the basis of $\{\mathbf{F}_+,\mathbf{F}_-\}$, and transition energies can be calculated using a simple *singlet-triplet* formula,[12,29]

$$\Omega_{ij}^{\{+,-\}}\approx\sqrt{\omega_{ij}(\omega_{ij}+2\lambda_{ij}K_{ij,kl}^{\{+,-\}})}, \tag{51}$$

where Ω_{ij}^{+} and Ω_{ij}^{-} correspond to the singlet and triplet transitions, respectively. This approximation can be viewed as an attempt to correct Kohn-Sham excitation energies individually, without including correlations among different single-particle transitions. If the TDLDA corrections to Kohn-Sham transition energies are relatively small, we can simplify Eq. (51) by taking a linear expansion around ω_{ij},

$$\Omega_{ij}\approx\omega_{ij}+\lambda_{ij}K_{ij,kl}^{\{+,-\}} \tag{52}$$

Equation (52), also known as the *single-pole* approximation, is identical to the approximate TDLDA formula derived in Ref. 7.

III. RESULTS AND DISCUSSION

A. Excitation energies of atoms

To assess the accuracy of the TDLDA formalism, we computed excitation energies for several closed-shell atoms. Calculations were performed inside a spherical boundary domain with a radius of 15 a.u. For all atoms, we included at least 25 unoccupied states, which described transitions to both bound and continuum levels. We observed no noticeable change in the computed excitation energies and oscillator strengths upon further increase of the boundary domain or the number of unoccupied states included in calculations. The results of our calculations for the $^1S\rightarrow{}^1P$ singlet transitions are presented in Table II. Along with the transition energies calculated using the full-matrix TDLDA formalism [Eq. (27)], we include the values from the approximate singlet-triplet [Eq. (51)] and single-pole [Eq. (52)] formulas. The analysis of data in Table II leads us to the following conclusions: First, although all three TDLDA equations im-

TABLE II. Singlet $^1S \rightarrow {}^1P$ excitation energies of atoms. The energies were evaluated using the full-matrix TDLDA expression [Eq. (27)], as well as the approximate singlet-triplet [Eq. (51)] and single-pole [Eq. (52)] formulas. Experimental values are taken from Ref. 30. The time-independent Kohn-Sham transition energies ω^{KS} are included for comparison. $-\epsilon_{\mathrm{HOMO}}^{\mathrm{LDA}}$ and $\Omega_{ion}^{\mathrm{SCF}}$ are the negative values of the energies for the highest-occupied molecular orbitals (Kohn-Sham LDA "ionization" energies) and self-consistent LDA ionization potentials, respectively. All values are in eV.

Atom	Experiment	Full matrix	Singlet-triplet	Single pole	ω^{KS}	$-\epsilon_{\mathrm{HOMO}}^{\mathrm{LDA}}$	$\Omega_{ion}^{\mathrm{SCF}}$
Be	5.28	4.94	5.07	5.43	3.50	5.61	9.04
Mg	4.34	4.34	4.56	4.76	3.39	4.78	7.74
Ca	2.94	3.22	3.36	3.56	2.39	3.85	6.23
Sr	2.69	2.96	3.10	3.28	2.22	3.59	5.80
Zn	5.79	5.71	6.30	6.54	4.79	6.07	9.72
Cd	5.41	5.10	5.60	5.86	4.12	5.56	8.88

prove upon time-independent Kohn-Sham transition energies, the values obtained with the full-matrix formula are clearly the best. The full-matrix TDLDA excitation energies agree with experiment within 5–10 % for all atoms. Second, the discrepancy between the exact full-matrix and approximate singlet-triplet transition energies demonstrates the important role of correlation effects among single-electron excitations. These correlations are particularly large in case of the Zn and Cd atoms, where they are caused by the presence of *d* levels that are close in energy to the valence electronic states. Third, our values calculated with the single-pole formula closely reproduce the TDLDA singlet excitation energies reported in Ref. 7. Poor agreement between these values and experiment has led the authors of Ref. 7 to the conclusion that the TDLDA formalism is not accurate because of the intrinsic errors associated with the local density approximation. In particular, the authors of Ref. 7 have attributed the discrepancy to the wrong asymptotic tail behavior of the LDA potential, which decays exponentially, whereas the exact potential should fall off as $\sim -1/r$. However, our calculations show that the observed discrepancy should be attributed to the inaccuracy of the single-pole formula itself, rather than to a principal failure of TDLDA. A similar conclusion about the limitations of the single-pole approximation has been made in the work of van Gisbergen *at al.*[31] As such, we find the asymptotic behavior of the potential to be of less importance for the low-energy excitations than was previously thought. Our observations agree with the majority of other TDLDA calculations for atoms and small molecules,[32,28] which demonstrate that despite the wrong asymptotic behavior of the potential, TDLDA often works remarkably well in the limit of lower transition energies.

In Table III we compare the singlet $^1S \rightarrow {}^1P$ and triplet $^1S \rightarrow {}^3P$ atomic excitation energies, calculated with different techniques. The comparison indicates that TDLDA transition energies are in better general agreement with experiment than the values obtained with either the optimized effective potential (OEP) or the self-consistent field (SCF) method.[7] The singlet OEP excitation energies in Table III are almost as accurate as those calculated with TDLDA. However, the TDLDA values for triplet transitions are much better than the corresponding OEP energies due to the fact that the exchange-only OEP method does not account for correlation effects, which are believed to be important for triplets.[33] The TDLDA values for both singlets and triplets are also superior to the ordinary self-consistent excitation energies. At the same time, the TDLDA method is more efficient than the SCF approach, since TDLDA requires only a single self-consistent calculation to obtain the entire excitation spectrum.

B. Absorption spectra of sodium clusters

We applied the TDLDA technique to calculate absorption spectra of small Na_n clusters. We selected sodium clusters because of the availability of a large body of experimental data related to their optical properties.[34,35] Ground-state structures for the clusters of interest were determined by Langevin simulated annealing, followed by minimization of forces.[36] To obtain more accurate cluster geometries, the final structural optimization was performed with the generalized gradient approximation for the exchange-correlation

TABLE III. Singlet and triplet excitation energies of atoms, calculated with TDLDA [Eq. (27)], optimized effective potential (OEP), and the self-consistent field (SCF) methods (Ref. 7). OEP energies of Ref. 7 were calculated using the single-pole formula [Eq. (52)]. Experimental triplet transition energies are averaged over different spin-orbit components. All values are in eV.

Atom	Transition	Experiment	TDLDA	OEP	SCF
Be	$^1S \rightarrow {}^1P$	5.28	4.94	5.33	4.50
	$^1S \rightarrow {}^3P$	2.72	2.45	1.88	2.46
Mg	$^1S \rightarrow {}^1P$	4.34	4.34	4.45	4.07
	$^1S \rightarrow {}^3P$	2.72	2.79	2.05	2.80
Ca	$^1S \rightarrow {}^1P$	2.94	3.22	3.18	2.87
	$^1S \rightarrow {}^3P$	1.89	1.93	1.22	1.96
Sr	$^1S \rightarrow {}^1P$	2.69	2.96	2.86	2.62
	$^1S \rightarrow {}^3P$	1.82	1.82	1.10	1.84
Zn	$^1S \rightarrow {}^1P$	5.79	5.71	5.74	5.48
	$^1S \rightarrow {}^3P$	4.05	4.27	3.40	4.30
Cd	$^1S \rightarrow {}^1P$	5.41	5.10	5.11	4.71
	$^1S \rightarrow {}^3P$	3.88	3.69	2.87	3.70

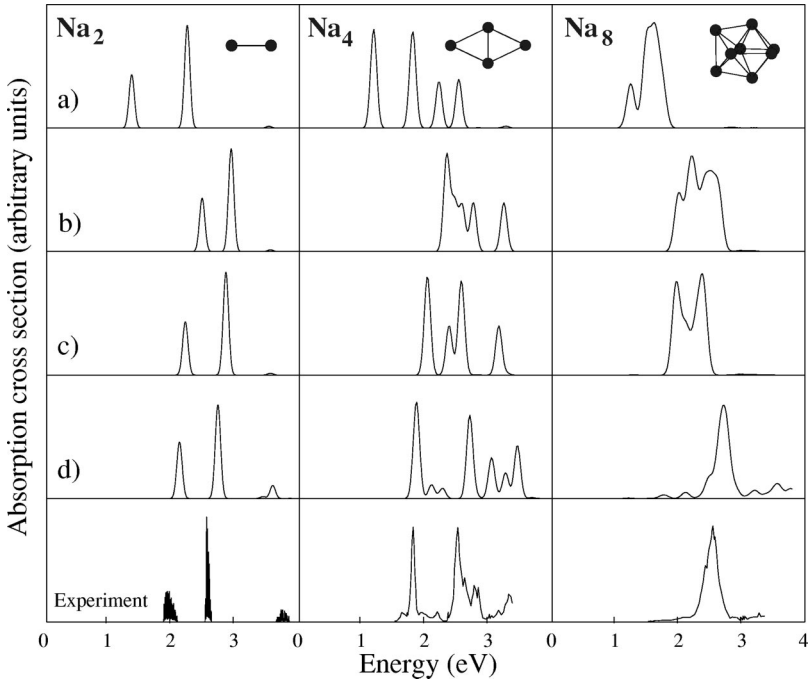

FIG. 3. Calculated and experimental absorption spectra of Na_2, Na_4, and Na_8 clusters. (a) Time-independent Kohn-Sham absorption spectra. The other plots show the TDLDA spectra calculated with (b) the single-pole approximation [Eq. (52)], (c) the singlet-triplet approximation [Eq. (51)], and (d) the full-matrix formula [Eq. (27)]. Experimental spectra are adapted from Ref. 35. A Gaussian convolution of 0.06 eV was used to simulate finite broadening of all calculated spectra.

potential.[37] Our structures for the Na_3 to Na_8 clusters agree with those reported previously[38] and all bond lengths agree to within $\sim 1\%$. The calculated interatomic distance of 3.08 Å for the Na_2 dimer is in excellent agreement with the experimental value of 3.0789 Å.[39] Since wave functions for unoccupied electronic states are very sensitive to the boundary conditions, TDLDA calculations need to be performed in a relatively large boundary domain. For sodium clusters, we used a spherical domain with a radius of 25 a.u. and a grid spacing of 0.8 a.u. We carefully tested for convergence of the calculated TDLDA excitation energies with respect to these parameters and with respect to the number of unoccupied states included in the calculation of the coupling matrix.

Calculated absorption spectra of three closed-shell clusters Na_2, Na_4, and Na_8 are shown in Fig. 3. In all cases, the time-independent Kohn-Sham LDA calculations substantially underestimate the energies of optical transitions. Of the three different TDLDA expressions, only the spectra calculated with the full matrix formula given by Eq. (27) agree with experiment. The large discrepancy between the exact [Fig. 3(d)] and the approximate [Fig. 3(c)] TDLDA spectra implies a significant degree of correlation among single-electron transitions. The role of correlation effects increases with increasing cluster size. When all electronic correlation effects are included, agreement between TDLDA and experiment is quite remarkable: The full-matrix TDLDA formalism correctly reproduces the experimental spectral shapes, and the calculated peak positions agree with experiment to within 0.1–0.2 eV. The comparison with other theoretical work reveals a close similarity between our full-matrix TDLDA spectra and the results of CI calculations.[40] Furthermore, our TDLDA spectrum for the Na_4 cluster better agrees with experiment than the GW absorption spectrum.[41] Calculated spectra of other Na_n clusters with $n<8$ are shown in Fig. 4. Again, the full-matrix TDLDA method greatly improves the quality of computed optical spectra with respect to the time-independent LDA calculations. The TDLDA spectra for Na_5, Na_6, and Na_7 closely match the available experimental measurements. A somewhat poorer agreement between experiment and the calculated absorption spectrum of Na_3 could be explained by the ''floppy'' structure of this cluster, i.e., the absence of a single pronounced minimum in its potential energy surface.[37] The lack of the stable ground-state structure for Na_3 makes its absorption spectrum more sensitive to temperature. The possible influence of experimental cluster temperature was not accounted for by our static TDLDA calculations and could be responsible for the observed disagreement.

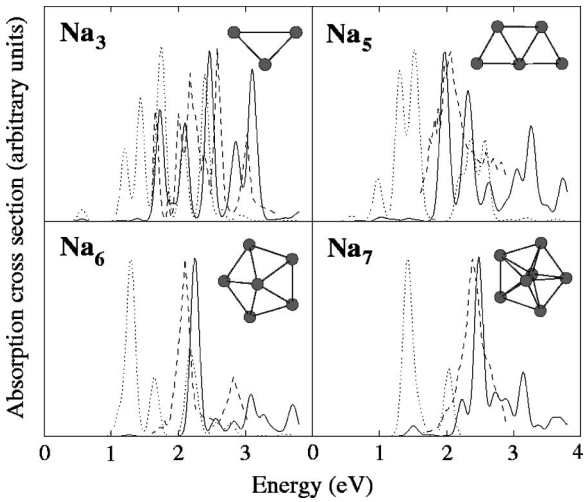

FIG. 4. Absorption spectra of Na_3, Na_5, Na_6, and Na_7 clusters. The TDLDA spectra (solid lines) were calculated with the full-matrix equation (27). The time-independent Kohn-Sham spectra (dotted lines) are shown for comparison. Experimental spectra (dashed lines) are adapted from Ref. 35. All calculated spectra are broadened by 0.06 eV.

TABLE IV. Energies and oscillator strengths of selected transitions in the absorption spectra of sodium clusters. Experimental transition energies are adapted from Ref. 35. Kohn-Sham LDA ''ionization'' energies $-\epsilon_{\mathrm{HOMO}}^{\mathrm{LDA}}$ and self-consistent LDA ionization potentials $\Omega_{ion}^{\mathrm{SCF}}$ are given as a reference. The assignment of the higher-energy excitations for Na_3 is somewhat ambiguous and these excitations are simply listed in ascending order. All energies are in eV.

Cluster	Experimental transition energy	TDLDA Energy	TDLDA Oscillator strength	$-\epsilon_{\mathrm{HOMO}}^{\mathrm{LDA}}$	$\Omega_{ion}^{\mathrm{SCF}}$
Na_2	1.91	2.10	0.64	3.21	5.17
	2.52	2.71	1.06		
	3.71	3.58	0.15		
Na_3	1.67	1.73	0.43	2.47	4.29
	2.05	2.09	0.37		
	2.21	2.47	0.62		
	2.59	2.85	0.25		
	3.02	3.10	0.48		
Na_4	1.80	1.85	1.03	2.77	4.38
	1.95	2.09	0.15		
	2.18	2.27	0.11		
	2.51	2.70	0.88		
	2.81	3.04	0.40		
Na_5	2.04[a]	1.97	1.10	2.61	4.26
		2.26	0.22		
		2.33	0.64		
		2.63	0.25		
Na_6	2.07	2.25	2.86	3.08	4.55
		2.55	0.25		
		2.83	0.24		
	2.85	3.08	0.66		
Na_7		1.50	0.14	2.58	4.20
		2.23	0.50		
	2.43[a]	2.48	2.42		
		2.73	0.46		
		2.87	0.36		
		2.95	0.22		
Na_8		1.79	0.08	3.09	4.52
		2.11	0.20		
		2.63	0.66		
	2.55[a]	2.67	1.22		
		2.69	0.20		
		2.76	1.98		
		2.90	0.33		

[a]Experimental absorption spectra of Na_5, Na_7, and Na_8 show a single broad band composed of several transitions not resolved individually.

Table IV shows the energies and oscillator strengths of selected transitions in the calculated absorption spectra. As a reference, we include in Table IV the self-consistent ionization potentials and the energies of the highest-occupied Kohn-Sham LDA orbitals. The self-consistent vertical ionization potentials $\Omega_{ion}^{\mathrm{SCF}}$ are calculated as the differences between the total energies of the neutral and the positively charged clusters, computed at the equilibrium atomic coordinates for the neutral clusters. The Kohn-Sham LDA ''ionization'' energies $-\epsilon_{\mathrm{HOMO}}^{\mathrm{LDA}}$ are given by the negative values of the energies for the highest-occupied LDA molecular orbitals. It has been shown that while TDLDA calculations usually provide good agreement with experiment for the excitation energies below $-\epsilon_{\mathrm{HOMO}}^{\mathrm{LDA}}$, they often tend to underestimate electronic excitation energies above this threshold.[28] Although the energies of many optical transitions listed in Table IV are close to, or even higher than $-\epsilon_{\mathrm{HOMO}}^{\mathrm{LDA}}$, the TDLDA energies for these transitions do not appear to be underestimated. The fact that the TDLDA formalism works relatively well beyond the region of its rigorous theoretical justification could be related to the specifics of optical absorption in sodium clusters: more than 95% of the total oscillator strength in their absorption spectra corresponds to transitions from bound to bound states. Consequently, transitions to continuum states, which are not well reproduced within TDLDA, do not contribute significantly to the spectra of Na_n clusters.

C. Optical absorption of benzene

While computational methods based on DFT are generally successful in predicting electronic properties of semiconductor and alkali metal clusters, organic molecules often pose more challenges for the density functional approach. The presence of localized chemical bonds in organic compounds leads to rapid spatial variations of the charge density that are difficult to describe within the DFT formalism. Because of that, the benzene molecule presents a more complex test for the TDLDA method than the systems we have considered so far. The experimental optical spectrum of benzene vapor is characterized by an extremely intense absorption peak near 6.9–7.0 eV, which corresponds to collective π-π^* transitions inside the aromatic hydrocarbon ring.[42] Recently, the optical spectrum of benzene was calculated using a *real-time* TDLDA method.[43] In contrast to our perturbation formalism in frequency space, the authors of Ref. 43 computed optical response in real time, by solving explicitly the time-dependent Schrödinger equation (8). Reference 43 reports good agreement between the real-time TDLDA calculations and experiment.

The ground-state structure of the benzene molecule was determined by LDA calculations. To minimize interatomic forces, we used a grid spacing of 0.3 a.u. and a boundary domain with a radius of 10 a.u. The calculated C—C (1.38 Å) and C—H (1.09 Å) bond lengths were in very good agreement with the experimental values of 1.399 Å and 1.101 Å, respectively. For the calculation of the TDLDA optical response we increased the radius of the boundary domain up to 15 a.u. and used a grid spacing of 0.4 a.u. The coupling matrix included transitions between 15 occupied and 45 unoccupied states.

Calculated and experimental absorption spectra are shown in Fig. 5. The time-independent Kohn-Sham calculations substantially underestimate the transition energy of the main π-π^* absorption peak for benzene. The TDLDA calculations

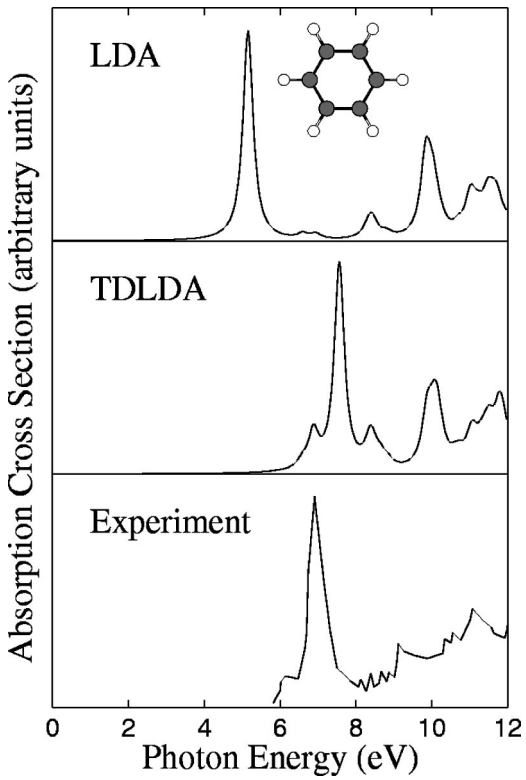

FIG. 5. Calculated and experimental optical spectra of benzene. The time-independent LDA spectrum (top) relates to the single-electron Kohn-Sham transitions. The TDLDA spectrum (middle) is based on Eq. (27). The experimental spectrum (bottom) is adapted from Ref. 42. Theoretical spectra are broadened by 0.1 eV. The Kohn-Sham LDA "ionization" energy of C_6H_6 is 6.53 eV and the self-consistent ionization potential is 9.54 eV.

produce a significant blue shift of the π-π^* peak and greatly improve agreement with experiment. Our spectrum also agrees well with the real-time TDLDA calculations.[43] We are encouraged that despite considerable differences in the computational approach both TDLDA methods produce similar results.

D. Absorption spectra of semiconductor clusters

Small semiconductor clusters exhibit properties remarkably different from those of bulk materials.[44] Understanding the nature of these differences presents a challenging problem. The lack of reliable experimental tools and limitations of theoretical simulations make it difficult to study the properties of clusters. In many cases, experimental information about cluster structures is available only through indirect measurements, such as measurements of optical absorption.[35,45,46] In this regard, theoretical calculations for absorption spectra of clusters are important, because they offer the potential for a straightforward comparison of theory and experiment.

For our calculations, we selected two semiconductor materials: silicon and gallium arsenide. As before, we used Langevin simulated annealing, followed by minimization of forces[36] to find ground-state structures for the clusters of interest. During the annealing, clusters were deposited inside a spherical domain with a radius of 13 a.u. The mesh size of the imposed grid was taken to be 0.7 a.u., although at the final stages of the structural relaxation we used a grid spacing of 0.4 a.u. to resolve the energies of quasidegenerate isomers. The choice of these parameters was justified by the fact that no significant changes in the total energy and the interatomic forces were detected with a further increase of the radius of the boundary sphere or decrease of the grid spacing. The calculated interatomic distance of 2.20 Å for the Si_2 dimer was close to the experimental bond length of 2.246 Å.[39] For the $X^3\Sigma^-$ ground state of the GaAs diatomic molecule[47] our equilibrium bond length of 2.51 Å was in agreement with the experimental value of 2.53 Å.[48] Optimized ground-state geometries of Si_n clusters containing up to ten atoms are shown in Fig. 6. For the most part, our cluster structures agree with those predicted by other *ab initio* calculations.[49] For example, in agreement with previous calculations,[36] we found two quasidegenerate isomers for the Si_6 cluster. Because of a large number of possible stoichiometries, the geometries of Ga_nAs_m were determined only for clusters with an almost equal number of gallium and arsenic atoms ($n=m, n=m\pm1$). Optimized ground-state structures of Ga_nAs_m clusters are shown in Fig. 7. These structures often resemble slightly distorted geometries of Si_n clusters with alternating Ga and As atoms. In two cases, we discovered two quasidegenerate isomers: for Ga_4As_4 the total energies of a bicapped octahedron and a tetracapped tetrahedron [the structures (I) and (II) as shown in Fig. 7] coincided within 0.02 eV, and for Ga_5As_5 the energy of a tetracapped trigonal prism (I) was only by 0.05 eV higher than that of a previously suggested structure[50] (II). Since TDLDA calculations are sensitive to the boundary conditions, we carefully tested for convergence of the computed excitation energies and absorption spectra with respect to the size of the bound-

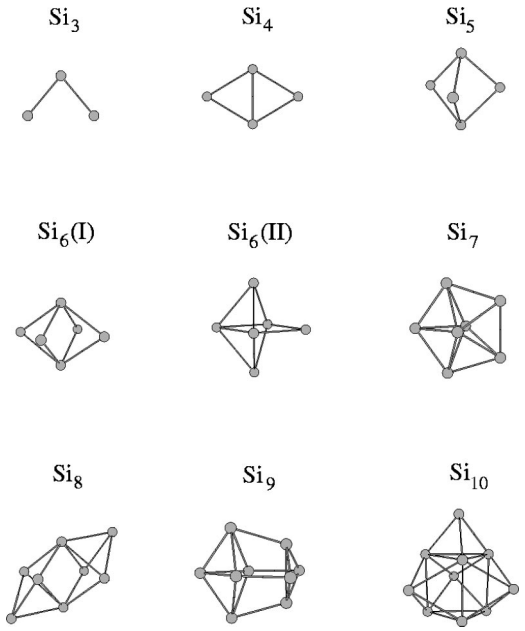

FIG. 6. Structures of Si_n clusters. Two quasidegenerate isomers are shown for Si_6.

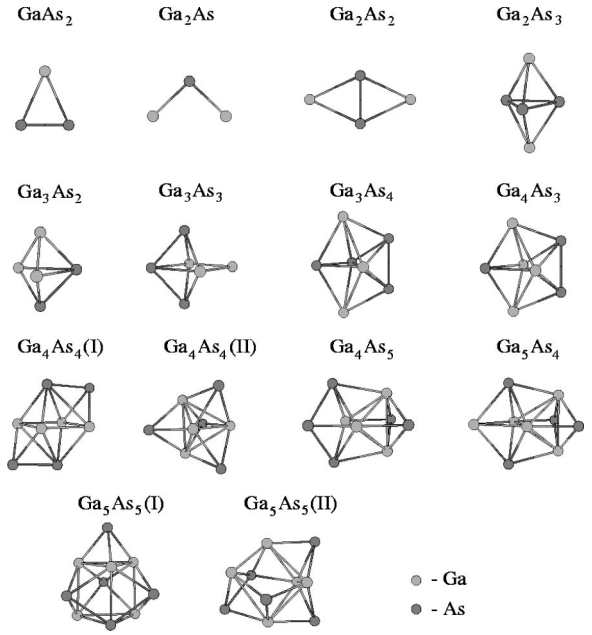

FIG. 7. Structures of Ga_nAs_m clusters. Quasidegenerate isomers are shown for Ga_4As_4 and Ga_5As_5.

ary domain, the grid spacing, and the total number of unoccupied single-electron states included in the TDLDA formalism. Based on the results of our convergence test, the final TDLDA calculations were performed using a boundary sphere with a radius of 21 a.u. and a grid spacing of 0.8 a.u. The number of unoccupied states included in the calculation of the TDLDA coupling matrix was taken to be at least 3 to 5 times greater than that of occupied states.

Figures 8 and 9 show the calculated TDLDA absorption spectra of Si_n and Ga_nAs_m clusters, respectively. For comparison, both plots also show the spectra of time-independent Kohn-Sham LDA eigenvalues. For all silicon and gallium arsenide clusters the TDLDA spectra display a substantial blue shift with respect to the Kohn-Sham eigenvalue spectra. The differences between the TDLDA and time-independent LDA spectra become more profound as the size of clusters increases. Our calculations also predict a substantial variety of spectral shapes for different clusters. It implies that clusters can be uniquely identified by their absorption spectra. In some cases, even for clusters of the same chemical composition, such as Ga_4As_4 (I) and (II), TDLDA calculations predict easily distinguishable spectra. This demonstrates a high sensitivity of the calculated optical spectra to cluster geometries and suggests that a comparison of calculated and experimental spectra can help identify isomers.

Practically all calculated TDLDA spectra for silicon and gallium arsenide clusters exhibit long absorption tails extending deep into the region of lower transition energies. Such behavior is noticeably absent in the optical absorption of semiconductor quantum dots and cannot be described in terms of a simple quantum confinement theory.[51,52] Quantum dots are truncated fragments of the bulk structure that are passivated at the boundaries.[53] Unlike the clusters considered in this section, they do not possess free surfaces. On this basis, we believe that the low-energy absorption can be attributed to the existence of free surfaces in the clusters. These results appear to be consistent with calculations for the static polarizabilities of semiconductor clusters, which show a significant surface contribution toward cluster polarizabilities. According to the sum-over-states formula for the average static polarizability, $\langle \alpha \rangle = \Sigma_I f_I / \Omega_I^2$, the presence of low-energy transitions in absorption spectra increases polarizabilities. This effect, in agreement with our previous calculations,[54] leads to higher polarizabilities for open-surface clusters as compared to that of quantum dots.

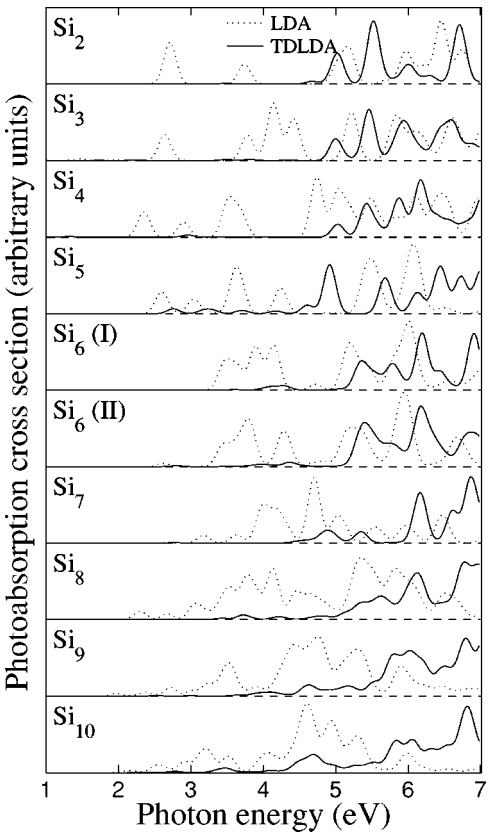

FIG. 8. Calculated TDLDA absorption spectra of silicon clusters (solid lines). The spectra of time-independent Kohn-Sham LDA eigenvalues (dotted lines) are shown for comparison. All TDLDA spectra are presented on the same relative scale. The Kohn-Sham eigenvalue spectra are scaled to fit in the same plot. A Gaussian convolution of 0.1 eV was used to simulate finite broadening of the calculated spectra.

The optical absorption gap in clusters and molecules can be defined naturally as the energy of the first dipole-allowed transition in the excitation spectrum. Unfortunately, this definition is difficult to apply in cases when the intensity of the first allowed excitation is too weak to be directly detected in experiment. In reported measurements for the optical absorption of gallium arsenide clusters[46] the problem of a limited experimental sensitivity was solved by defining an *effective* optical gap $\Omega_g(p)$ at a small but nonzero fraction of the integral oscillator strength,

$$\int_0^{\Omega_g(p)} \sigma(\omega) d\omega = p f_e, \tag{53}$$

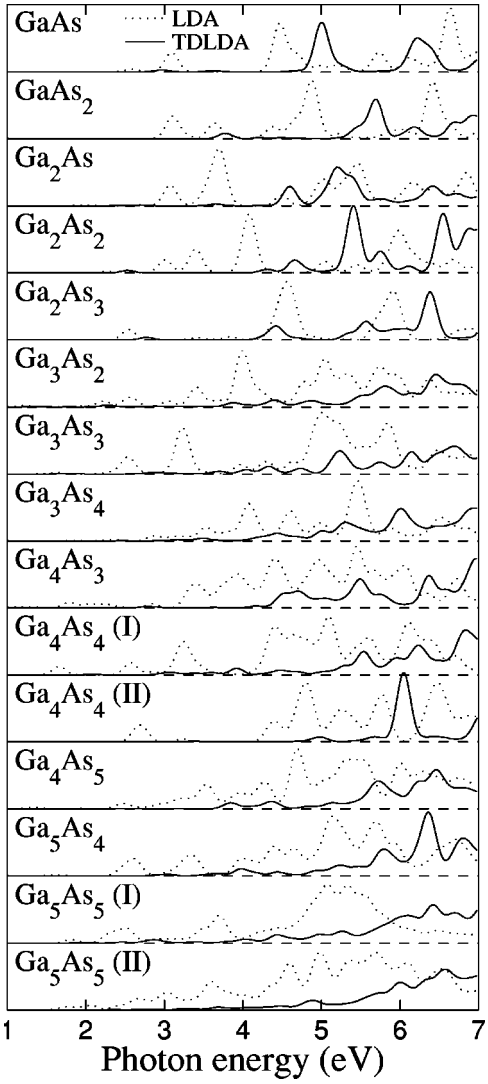

FIG. 9. Calculated TDLDA (solid lines) and time-independent LDA (dotted lines) absorption spectra of gallium arsenide clusters. The time-independent LDA spectra are scaled to fit in the same plot. All spectra are broadened by 0.1 eV using a Gaussian convolution.

where $\sigma(\omega)$ is the photoabsorption cross section per electron, f_e is the complete one-electron oscillator strength,[55] $f_e = 2\pi^2\hbar e^2/mc \cong 1.098$ eV Å^2, and p is a small positive number. In the experimental work of Ref. 46 the value of this parameter was taken to be $p = 0.02$.

Photoabsorption gaps for silicon and gallium arsenide clusters are given in Tables V and VI. Theoretical gaps were computed at $p = 0.02$ and $p \to 0$. For practical reasons, the $p \to 0$ limit was calculated by setting the value of this threshold parameter to 10^{-4}. The chosen value of 10^{-4} stands above the level of numerical "noise," but is sufficiently small as to not suppress dipole-allowed transitions. Regardless of the value of the onset parameter p, the time-independent LDA calculations always severely underestimate the experimental photoabsorption gaps for gallium arsenide clusters. For the TDLDA absorption, however, the presence of long and low intensity tails in the optical spectra results in substantial differences between the gaps estimated

TABLE V. Photoabsorption gaps and ionization thresholds of silicon clusters. All values are in eV.

	LDA		TDLDA			
Cluster	$p \to 0$	$p = 0.02$	$p \to 0$	$p = 0.02$	$-\epsilon_{\mathrm{HOMO}}^{\mathrm{LDA}}$	$\Omega_{ion}^{\mathrm{SCF}}$
Si_2	2.71	2.71	3.49	5.03	5.41	7.93
Si_3	0.88	2.64	2.23	5.46	5.46	8.23
Si_4	2.35	2.35	2.96	5.42	5.61	8.14
Si_5	2.55	2.58	2.74	4.92	5.88	8.32
Si_6 (I)	3.46	3.46	3.99	5.52	5.70	7.99
Si_6 (II)	2.62	3.43	3.74	5.50	5.67	7.99
Si_7	2.66	3.18	4.46	6.13	5.86	8.12
Si_8	2.30	2.68	3.44	5.57	5.31	7.40
Si_9	1.96	2.71	3.49	5.77	5.63	7.72
Si_{10}	2.12	2.54	2.81	5.58	6.04	8.02

at $p = 0.02$ and $p \to 0$. As expected, the $p \to 0$ TDLDA gaps for gallium arsenide clusters appear to be much smaller than the experimental values of Ref. 46. At the same time, for the majority of our clusters we find the photoabsorption gaps defined as in the experimental work at $p = 0.02$ to be in good agreement with experiment. We also note that for the diatomic GaAs molecule our $p \to 0$ TDLDA gap of 2.97 eV is very close to the experimental energy of 2.92 eV for the lowest allowed electronic transition $^3\Pi \leftarrow X^3\Sigma^-$.[56]

Tables V and VI also include the self-consistent ionization potentials and the energies of the highest-occupied Kohn-Sham LDA orbitals. For a number of clusters, TDLDA photoabsorption gaps calculated at $p = 0.02$ appear to be close to $-\epsilon_{\mathrm{HOMO}}^{\mathrm{LDA}}$, which raises a question about the reliability of TDLDA calculations in that region. However, the fact that the calculated $p = 0.02$ gaps for most gallium arsenide clusters agree well with experiment seems to indicate that the values of these gaps were not strongly affected by their proximity to the $-\epsilon_{\mathrm{HOMO}}^{\mathrm{LDA}}$.

The variation of the photoabsorption gaps for gallium arsenide clusters with cluster size is shown in Fig. 10. In all cases, the TDLDA gaps for clusters are greater than the absorption gap of bulk gallium arsenide. At the same time, our $p \to 0$ TDLDA gaps are much smaller than the typical gap values for semiconductor quantum dots in this size range.[51,52] In contrast to the case of quantum dots, we observe only a weak dependence of the gap value on cluster size. Our calculations predict smaller gaps for clusters that contain a higher fraction of gallium atoms. This is consistent with the fact that the excitation energy of atomic Ga is lower than that of As.[30] Due to the almost identical masses of the Ga and As atoms, the experimental measurements of Ref. 46 were performed on $n + m = \mathrm{const}$ ensembles of Ga_nAs_m clusters. In this respect, the observed discrepancy between the theoretical and experimental absorption gaps for $n + m = 4$ and 5 may indicate a greater share of the Ga-rich structures among very small gallium-arsenide clusters generated in the experiment.

E. Optical gaps in nanocrystalline silicon

The study of optical excitations in hydrogen-terminated silicon clusters is essential for understanding absorption and

TABLE VI. Photoabsorption gaps and ionization thresholds of gallium arsenide clusters. Experimental gaps are adapted from Ref. 46. All values are in eV.

	LDA		TDLDA		Experiment		
Cluster	$p\to 0$	$p=0.02$	$p\to 0$	$p=0.02$	$p=0.02$	$-\epsilon_{\mathrm{HOMO}}^{\mathrm{LDA}}$	$\Omega_{ion}^{\mathrm{SCF}}$
GaAs	2.59	3.09	2.97	4.95		4.99	7.68
$GaAs_2$	1.02	3.10	3.74	5.43		4.78	7.77
Ga_2As	1.94	3.07	2.42	4.59		5.24	8.09
Ga_2As_2	2.27	3.01	2.53	5.09	3.6 ± 0.2	5.23	7.63
Ga_2As_3	2.55	2.55	2.78	5.57	4.3 ± 0.3	4.87	7.52
Ga_3As_2	1.20	2.53	2.28	4.94		5.10	7.59
Ga_3As_3	1.20	2.51	2.86	5.24	5.5 ± 0.3	5.45	7.69
Ga_3As_4	1.79	2.87	3.12	5.26	5.0 ± 0.4	4.20	6.63
Ga_4As_3	0.90	2.04	1.59	4.90		4.97	7.31
Ga_4As_4 (I)	1.66	2.57	3.00	5.53	5.2 ± 0.2	4.60	6.67
Ga_4As_4 (II)	0.94	2.67	3.15	6.04		5.70	7.78
Ga_4As_5	1.21	2.90	2.47	5.67	5.1 ± 0.2	4.76	6.88
Ga_5As_4	0.93	2.54	3.06	5.62		5.09	7.24
Ga_5As_5 (I)	0.93	2.30	2.59	5.61	5.1 ± 0.2	5.74	7.72
Ga_5As_5 (II)	1.75	2.60	2.75	5.69		5.55	7.53

emission of visible light in porous silicon and quantum dots.[58] Over the last decade, Si_nH_m clusters in the form of quantum dots have been the subject of intensive experimental[59–61] and theoretical[52,53,62–67] research. However, disagreements among different theoretical models used for describing electronic excitations in these systems remain a subject of significant controversy. For the most part, the disagreements arise from the formulation of the optical gap in confined systems and the calculation of different components, such as image charges, self-energies and excitonic contributions that comprise the optical gap.[68,69]

Most theoretical studies focus primarily on the size dependence of photoluminescence energies and photoabsorption gaps.[53,62–67] In many cases, such calculations do not evaluate oscillator strengths and cannot explicitly identify optically allowed and dark transitions. This creates an uncertainty in the theoretical interpretation of the experimentally measured optical absorption. Only one of the published works[52] presents calculations for the entire absorption *spectra* of a few small ($n+m\leqslant 34$) Si_nH_m clusters. The lack of theoretical studies dealing with the optical spectra for larger clusters can be explained by the extreme complexity of such calculations, e.g., the difficulty in describing many-body effects in confined systems. TDLDA represents a fully *ab initio* formalism for excited states. It is not constrained to a single electronic transition, but explicitly evaluates oscillator strengths for all transitions in the vicinity of the absorption gap. As such, our calculations are removed from the theoretical disagreements mentioned above. Unlike time-independent LDA calculations for clusters, the TDLDA approach does not require any additional artificial adjustment of the obtained electronic excitation energies and absorption gaps.

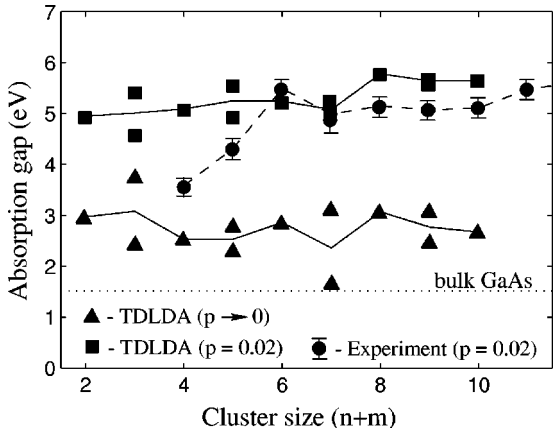

FIG. 10. Calculated and experimental photoabsorption gaps of Ga_nAs_m clusters vs cluster size. The TDLDA gaps are shown for $p\to 0$ and $p=0.02$. For clusters with an odd number of atoms the solid lines are drawn through the midpoint between the gaps of Ga-rich and As-rich structures. The dotted line corresponds to the absorption gap of bulk gallium arsenide.[57]

Structures of Si_nH_m clusters were obtained by starting with the coordinates of bulk silicon and minimizing the interatomic forces acting on silicon and hydrogen atoms. We completely optimized the structures of all clusters up to $Si_{35}H_{36}$. Larger clusters were built by using spherical fragments of the LDA-optimized silicon bulk lattice and further relaxing the outer layers by minimizing forces acting on the surface hydrogen atoms. The structures of selected Si_nH_m clusters are shown in Fig. 11. Before proceeding with TDLDA calculations, we carefully tested the computed excitation energies and absorption spectra for convergence. For all clusters, we required at least a 10–12 a.u. separation between the surface atoms and the boundary of the computational domain. In the calculation of the TDLDA transition matrix elements, we included at least two to three times as many unoccupied states as the number of occupied electronic

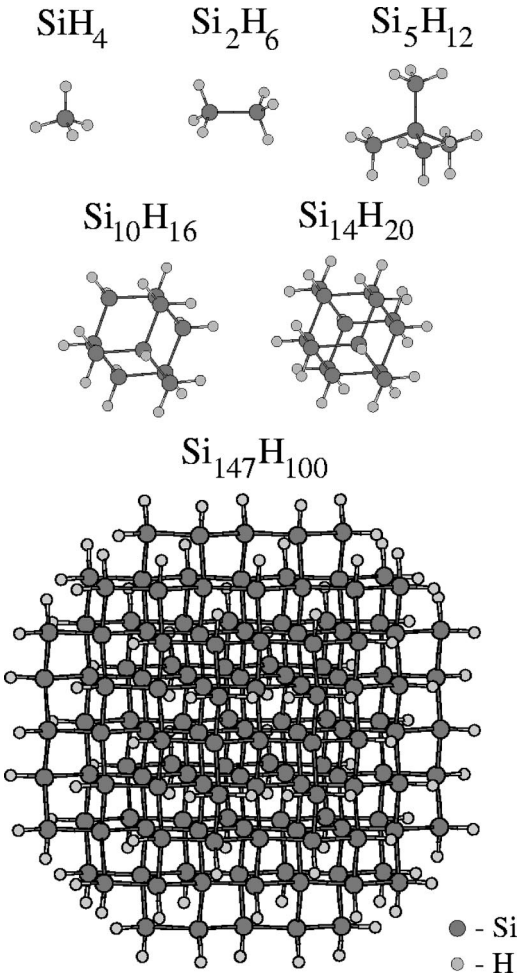

FIG. 11. Structures of Si_nH_m clusters.

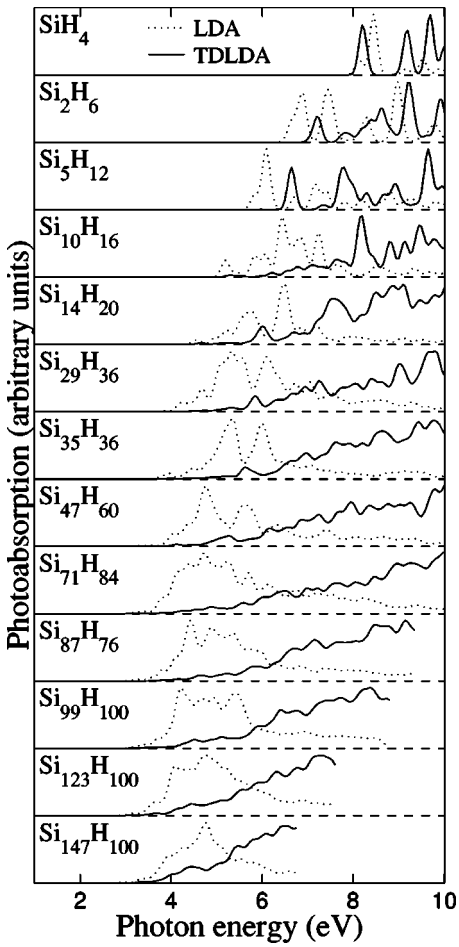

FIG. 12. Calculated TDLDA absorption spectra of Si_nH_m clusters (solid lines). Spectra of time-independent Kohn-Sham LDA eigenvalues (dotted lines) are shown for comparison. All spectra are broadened by 0.1 eV using a Gaussian convolution.

states. These conditions were sufficient to achieve convergence of the computed spectra in the experimentally important region below 10 eV.

The calculated absorption spectra of Si_nH_m clusters are shown in Fig. 12. To reduce the memory requirements and the overall computational load, spectra of the last four clusters were calculated including only electronic transitions below a chosen energy threshold. Along with the TDLDA spectra, we show the spectra of time-independent Kohn-Sham LDA eigenvalues. As in the case of metallic and semiconductor clusters with open surfaces, the TDLDA spectra of Si_nH_m clusters are blueshifted with respect to the Kohn-Sham eigenvalue spectra. Unlike optical spectra of ''bare'' semiconductor clusters considered in the preceding section, the spectra of hydrogenated silicon clusters do not display low-energy transitions associated with the surface states. Photoabsorption gaps for Si_nH_m clusters are much larger than those of Si_n clusters with open surfaces. As the size of clusters increases, the absorption gaps gradually decrease, and the discrete spectra for small clusters evolve into quasi-continuous spectra for silicon nanocrystals. Figure 13 demonstrates that the oscillator strength of dipole-allowed transitions near the absorption edge decreases with increasing cluster size. This fact is consistent with the formation of an *indirect* band gap in the limit of bulk silicon.[66]

In Table VII, we compare TDLDA values for the excitation energies of the first three Si_nH_m clusters with experimental data[59,66] as well as with the values calculated using the Bethe-Salpeter technique.[52] Table VII also shows the Kohn-Sham LDA ''ionization'' energies of the clusters, $-\epsilon_{\mathrm{HOMO}}^{\mathrm{LDA}}$, given by the negative values of the energies for the highest-occupied LDA electronic orbitals. The table demonstrates that the calculated TDLDA excitation energies for the transitions below or close to $-\epsilon_{\mathrm{HOMO}}^{\mathrm{LDA}}$ agree well with the experimental data and the Bethe-Salpeter values. This agreement, however, deteriorates for higher excitations, which lie above $-\epsilon_{\mathrm{HOMO}}^{\mathrm{LDA}}$. As the size of clusters increases, the energy of the first-allowed excitation moves further down from the LDA ''ionization'' energy, and the agreement with experiment improves. For large Si_nH_m clusters, the first-allowed optical transitions are always located below $-\epsilon_{\mathrm{HOMO}}^{\mathrm{LDA}}$. The LDA HOMO energy gradually diminishes from 6.8 eV for $Si_{10}H_{16}$ to 5.6 eV for $Si_{147}H_{100}$, but remains considerably larger than the values of the TDLDA absorption gaps. On this basis, we believe that TDLDA should provide an accurate description of the photoabsorption gaps and the low-energy optical transitions in larger Si_nH_m clusters.

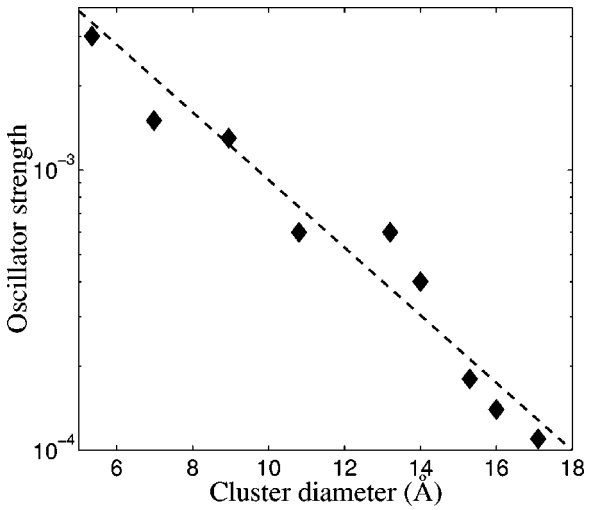

FIG. 13. Oscillator strength of dipole-allowed transitions near the absorption edge vs cluster diameter.

The optical absorption gaps for small clusters can be defined directly by the energy of the first dipole-allowed transition in their absorption spectra. For large clusters, the absorption spectra become essentially quasicontinuous. A large number of low-intensity transitions exist near the absorption edge. Taken individually, the oscillator strengths of these transitions would be located far below the experimentally detectable limit. As a result, identifying the first-allowed optical transition in the case of large clusters is not a trivial task. Rather than associating the optical gaps with the individual transitions, we define them through the integral oscillator strength according to Eq. (53). Similarly, as we did in case of Ga_nAs_m clusters, we calculate the photoabsorption gaps for Si_nH_m clusters in the limit of $p \rightarrow 0$ by setting the actual value of this threshold parameter to 10^{-4}. Defining the absorption gaps in such a way does not affect the values of the optical gaps for small Si_nH_m clusters, since the intensity of their first-allowed transitions is much higher than the selected threshold. At the same time, Eq. (53) offers a convenient way for the evaluation of optical gaps in large clusters, which is consistent with methods commonly used in experimental work.

TABLE VII. Excitation energies of hydrogenated silicon clusters. The experimental optical absorption energies are taken from Ref. 59 (silane and disilane), and Ref. 66 (neopentasilane). The assignment of electronic excitations for silane and disilane corresponds to the Rydberg transitions. The Bethe-Salpeter (BS) excitation energies are adapted from Ref. 52. $-\epsilon_{\mathrm{HOMO}}^{\mathrm{LDA}}$ are Kohn-Sham LDA ''ionization''energies and $\Omega_{ion}^{\mathrm{SCF}}$ are self-consistent LDA ionization potentials. All values are in eV.

Cluster	Transition	Experiment	BS	TDLDA	$-\epsilon_{\mathrm{HOMO}}^{\mathrm{LDA}}$	$\Omega_{ion}^{\mathrm{SCF}}$
SiH_4	4*s*	8.8	9.0	8.2	8.6	12.3
	4*p*	9.7	10.2	9.2		
	4*d*	10.7	11.2	9.7		
Si_2H_6	4*s*	7.6	7.6	7.3	7.5	10.8
	4*p*	8.4	9.0	7.8		
Si_5H_{12}		6.5	7.2	6.6	7.3	9.6

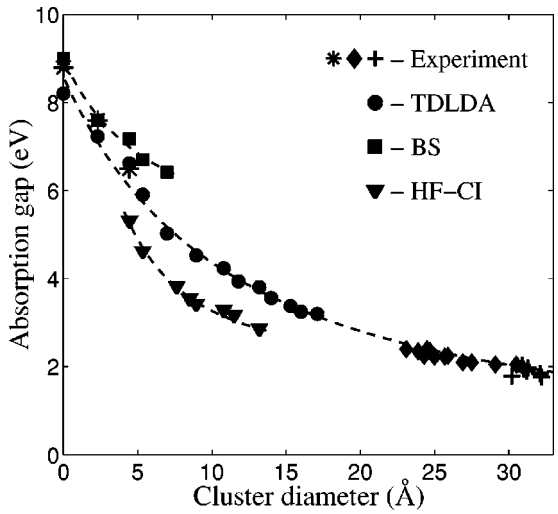

FIG. 14. Variation of optical absorption gaps as a function of cluster diameter. Theoretical values shown in the plot include the gaps calculated by the TDLDA method (this paper), by the Bethe-Salpeter (BS) technique (Ref. 52), and by the Hartree-Fock method with the correlation included through the configuration-interaction approximation (HF-CI) [Ref. 67]. Experimental values are taken from Refs. 59, 60, and 66. The dashed lines are a guide to the eye.

The variation of the optical absorption gaps as a function of the cluster size is shown in Fig. 14. Along with the TDLDA values, we included optical gaps calculated by the Bethe-Salpeter (BS) technique.[52] For very small clusters, SiH_4, Si_2H_6, and Si_5H_{12}, the gaps computed by the TDLDA method are close to the BS values, although for $Si_{10}H_{16}$ and $Si_{14}H_{20}$ our gaps are considerably smaller than the BS gaps. At the same time, our TDLDA gaps for clusters in the size range from 5 to 71 silicon atoms are larger by ~ 1 eV than the gaps calculated by the Hartree-Fock technique with the correlation correction included through the configuration-interaction approximation (HF-CI).[67] These differences are consistent with the fact that the BS calculations systematically overestimate and the HF-CI calculations of Ref. 67 underestimate the experimental absorption gaps. For example, for the optical absorption gap of Si_5H_{12} the BS, TDLDA, and HF-CI methods predict the values of 7.2, 6.6, and 5.3 eV, respectively, compared to the experimental value of 6.5 eV. However, it is not clear whether the gaps of Ref. 67 refer to the optically allowed or optically forbidden transitions, which may offer a possible explanation for the observed discrepancy. In the limit of large clusters, we find the TDLDA optical gaps to be in generally good agreement with the photoabsorption gaps evaluated by the majority of self-energy corrected LDA (Refs. 53 and 66) and empirical[64,65] techniques. At present, the full TDLDA calculations for clusters larger than 20 Å in diameter remain beyond our capabilities. Nevertheless, the extrapolation of the TDLDA curve in the limit of large clusters comes very close to the experimental values for the photoabsorption gaps.

It is well known that time-independent LDA calculations typically underestimate the experimental photoabsorption gaps. Recent calculations for the frequency-dependent dielectric function in crystals[70] suggest that TDLDA and LDA

gaps might converge for an infinite system. We did not observe this trend for the clusters we have examined in our work. On the contrary, for all clusters considered, our calculations show a substantial difference between the optical spectra and photoabsorption gaps calculated by the TDLDA and the time-independent LDA methods. We do not rule out the possibility that the TDLDA optical transitions will converge with the regular time-independent LDA spectra for much larger systems. Nevertheless, our calculations suggest that such convergence does not occur at least up to several hundred atoms, which is sufficient for a large variety of prospective TDLDA applications. As such, it is not necessary to invoke *ad hoc* empirical assumptions to examine systems comparable in size to experimentally measured quantum dots.[65]

IV. CONCLUSIONS

We have implemented linear-response theory within the *time-dependent* density-functional formalism and the local-density approximation (TDLDA) to compute excitation energies and optical absorption spectra of atomic clusters. The calculated TDLDA excitation energies and absorption spectra for atoms, semiconductor and metallic clusters, and hydrogen-terminated silicon dots were found to be in good agreement with the experiment. The comparison of the spectra calculated with the exact and the approximate TDLDA expressions indicates an important role of collective electronic effects. The structural sensitivity of the calculated optical spectra for clusters suggests the possibility of using absorption spectra to identify clusters and separate isomers.

We have shown that the TDLDA formalism can provide an efficient alternative to more complex theoretical methods for excited state properties. Compared to other first-principles techniques for excited states, the TDLDA method requires considerably less computational effort and can be used for much larger systems. At the same time, as a fully *ab initio* technique, TDLDA avoids many of the controversies associated with empirical or semiempirical methods. The *ab initio* nature of the TDLDA formalism makes it flexible in application to a variety of systems composed of different chemical elements.

ACKNOWLEDGMENTS

We acknowledge support for this work by the National Science Foundation, the United States Department of Energy, and Minnesota Supercomputing Institute. We also thank Leeor Kronik for useful discussions and help in revising the manuscript.

*Present address: Department of Physics, University of Illinois at Urbana-Champaign, Urbana, IL 61801.

[1] W. Andreoni and G. Pastore, Phys. Rev. B **41**, 10 243 (1990).

[2] P. Hohenberg and W. Kohn, Phys. Rev. **136**, B864 (1964); W. Kohn and L.J. Sham, Phys. Rev. **140**, A1133 (1965); W. Kohn and P. Vashishta, in *Theory of Inhomogeneous Electron Gas*, edited by S. Lundqvist and N. H. March (Plenum Press, New York, 1983).

[3] See, for example, M. L. Cohen and J. R. Chelikowsky, *Electronic Structure and Optical Properties of Semiconductors*, 2nd ed. (Springer-Verlag, Berlin, 1989); J. R. Chelikowsky and M. L. Cohen, in *Handbook on Semiconductors*, edited by T. S. Moss and P. T. Landsberg (Elsevier, Amsterdam, 1992); M.C. Payne, M.P. Teter, D.C. Allan, T.A. Arias, and J.D. Joannopoulos, Rev. Mod. Phys. **64**, 1045 (1992); W. Pickett, Comput. Phys. Rep. **9**, 115 (1989); G.P. Srivastava and D. Weaire, Adv. Phys. **36**, 463 (1987).

[4] J.R. Chelikowsky, N. Troullier, and Y. Saad, Phys. Rev. Lett. **72**, 1240 (1994); J.R. Chelikowsky, N. Troullier, K. Wu, and Y. Saad, Phys. Rev. B **50**, 11 355 (1994).

[5] B. Fornberg and D. M. Sloan, *Acta Numerica* (1994), pp. 203–267; G. D. Smith, *Numerical Solutions of Partial Differential Equation: Finite Difference Methods*, 2nd ed. (Oxford, New York, 1978).

[6] W. Andreoni, in *The Chemical Physics of Atomic and Molecular Clusters*, edited by G. Scoles (North-Holland, Amsterdam, 1990), pp. 159–175.

[7] E. K. U. Gross, J. F. Dobson, and M. Petersilka, in *Density Functional Theory*, edited by R. F. Nalewajski (Springer-Verlag, Berlin, 1996), p. 81; M. Petersilka, U.J. Gossmann, and E.K.U. Gross, Phys. Rev. Lett. **76**, 1212 (1996).

[8] V.R. Saunders and J.H. van Lenthe, Mol. Phys. **48**, 923 (1983); R.J. Buenker, S.D. Peyerimhoff, and W. Butscher, *ibid.* **35**, 771 (1978).

[9] D.M. Ceperley and B. Bernu, J. Chem. Phys. **89**, 6316 (1988); B. Bernu, D.M. Ceperley, and W.A. Lester, Jr., *ibid.* **93**, 552 (1990); **95**, 7782 (1991).

[10] L.J. Sham and T.M. Rice, Phys. Rev. **144**, 708 (1966); L. Hedin, Phys. Rev. **139**, A796 (1965).

[11] M. E. Casida, in *Recent Advances in Density-Functional Methods*, Part I, edited by D. P. Chong (World Scientific, Singapore, 1995), p. 155; in *Recent Developments and Applications of Modern Density Functional Theory*, edited by J. M. Seminario (Elsevier, Amsterdam, 1996), p. 391.

[12] I. Vasiliev, S. Öğüt, and J.R. Chelikowsky, Phys. Rev. Lett. **82**, 1919 (1999).

[13] X. Blase, A. Rubio, S.G. Louie, and M.L. Cohen, Phys. Rev. B **52**, R2225 (1995).

[14] I. Vasiliev, S. Öğüt, and J.R. Chelikowsky, Phys. Rev. B **60**, R8477 (1999).

[15] I. Vasiliev, S. Öğüt, and J.R. Chelikowsky, Phys. Rev. Lett. **86** 1813 (2001).

[16] B. Fornberg and D. M. Sloan, *Acta Numerica* (1994), p. 203; G. D. Smith, *Numerical Solutions of Partial Differential Equation: Finite Difference Methods*, 2nd ed. (Oxford, New York, 1978).

[17] L. Kleinman and D.M. Bylander, Phys. Rev. Lett. **48**, 1425 (1982).

[18] N. Troullier and J.L. Martins, Phys. Rev. B **43**, 1993 (1991).

[19] D.M. Ceperley, Phys. Rev. B **18**, 3126 (1978); D.M. Ceperley and B.J. Alder, Phys. Rev. Lett. **45**, 566 (1980).

[20] S.G. Louie, S. Froyen, and M.L. Cohen, Phys. Rev. B **26**, 1738 (1982).

[21] A. Stathopoulos, S. Öğüt, Y. Saad, J.R. Chelikowsky, and H. Kim, Comput. Sci. Eng. **2**, 19 (2000).

[22] R.B. Morgan and D.S. Scott, SIAM (Soc. Ind. Appl. Math.) J. Sci. Stat. Comput. **7**, 817 (1986).
[23] B.M. Deb and S.K. Ghosh, J. Chem. Phys. **77**, 342 (1982); S.K. Ghosh and B.M. Deb, Chem. Phys. **71**, 295 (1982); L.J. Bartolotti, Phys. Rev. A **24**, 1661 (1981); *ibid.* **26**, 2243 (1982); E. Runge and E.K.U. Gross, Phys. Rev. Lett. **52**, 997 (1984).
[24] E.K.U. Gross and W. Kohn, Phys. Rev. Lett. **55**, 2850 (1985); Adv. Quantum Chem. **21**, 255 (1990).
[25] G. D. Mahan, *Many-Particle Physics* (Plenum Press, New York, 1981), Chap. 5.
[26] J.P. Perdew and A. Zunger, Phys. Rev. B **23**, 5048 (1981).
[27] D.E. Beck, Phys. Rev. B **43**, 7301 (1991).
[28] C. Jamorski, M.E. Casida, and D.R. Salahub, J. Chem. Phys. **104**, 5134 (1996); M.E. Casida, C. Jamorski, K.C. Casida, and D.R. Salahub, *ibid.* **108**, 4439 (1998).
[29] T. Grabo, M. Petersilka, E.K.U. Gross, J. Mol. Struct.: THEOCHEM **501**, 353 (2000).
[30] C. E. Moore, *Atomic Energy Levels*, Natl. Bur. Stand. Ref. Data Ser. (U.S. GPO, Washington D.C., 1971), Vol. I–III.
[31] S. J. A. van Gisbergen, F. Kootstra, P.R.T. Schipper, O.V. Gritsenko, J.G. Snijders, and E.J. Baerends, Phys. Rev. A **57**, 2556 (1998).
[32] R. Bauernschmitt, M. Haser, O. Treutler, and R. Ahlrichs, Chem. Phys. Lett. **264**, 573 (1997); R. Bauernschmitt and R. Ahlrichs, *ibid.* **256**, 454 (1996).
[33] C.A. Ullrich, U.J. Gossmann, and E.K.U. Gross, Phys. Rev. Lett. **74**, 872 (1995); J.B. Krieger, Y. Li, and G.J. Iafrate, Phys. Rev. A **45**, 101 (1992).
[34] W.A. de Heer, Rev. Mod. Phys. **65**, 611 (1993); V. Bonačić-Koutecký, P. Fantucci, and J. Koutecký, Chem. Rev. **91**, 1035 (1991).
[35] C. R. C. Wang, S. Pollack, D. Cameron, and M.M. Kappes, J. Chem. Phys. **93**, 3787 (1990); Chem. Phys. Lett. **165**, 26 (1990); C.R.C. Wang, S. Pollack, T.A. Dahlseid, G.M. Koretsky, and M.M. Kappes, J. Chem. Phys. **96**, 7931 (1992); S.P. Sinha, Proc. Phys. Soc. London **62**, 124 (1949); W.R. Fredrickson and W.W. Watson, Phys. Rev. **30**, 429 (1927).
[36] X. Jing, N. Troullier, D. Dean, N. Binggeli, J.R. Chelikowsky, K. Wu, and Y. Saad, Phys. Rev. B **50**, 12 234 (1994)
[37] L. Kronik, I. Vasiliev, and J.R. Chelikowsky, Phys. Rev. B **62**, 9992 (2000); L. Kronik, I. Vasiliev, M. Jain, and J. R. Chelikowsky, J. Chem. Phys. **115**, 4322 (2001); *ibid.* **115**, 8714 (2001).
[38] P. Calaminici, K. Jug, and A.M. Köster, J. Chem. Phys. **111**, 4613 (1999).
[39] *CRC Handbook of Chemistry and Physics*, edited by D. R. Lide, 81st ed. (CRC Press, New York, 2000), pp. 9-17–9-43.
[40] V. Bonačić-Koutecký, P. Fantucci, and J. Koutecký, J. Chem. Phys. **93**, 3802 (1990); Chem. Phys. Lett. **166**, 32 (1990); V. Bonačić-Koutecký, J. Pittner, C. Scheuch, M.F. Guest, and J. Koutecký, J. Chem. Phys. **96**, 7938 (1992).
[41] G. Onida, L. Reining, R.W. Godby, R. Del Sole, and W. Andreoni, Phys. Rev. Lett. **75**, 818 (1995).
[42] E.E. Koch and A. Otto, Chem. Phys. Lett. **12**, 476 (1972).
[43] K. Yabana and G.F. Bertsch, Int. J. Quantum Chem. **75**, 55 (1999).
[44] M.F. Jarrold, Science **252**, 1085 (1991).
[45] See, for example, J. Blanc, V. Bonačić-Koutecký, M. Broyer, J. Chevaleyre, P. Dugourd, J. Koutecký, C. Scheuch, J.P. Wolf, and L. Wöste, J. Chem. Phys. **96**, 1793 (1992); K.D. Rinnen, K.D. Kolenbrander, A.M. DeSantolo, and M.L. Mandich, *ibid.* **96**, 4088 (1992); K.D. Rinnen and M.L. Mandich, Phys. Rev. Lett. **69**, 1823 (1992).
[46] R. Schäfer and J.A. Becker, Phys. Rev. B **54**, 10 296 (1996).
[47] U. Meier, S.D. Peyerimhoff, P.J. Bruna, and F. Grein, J. Mol. Spectrosc. **134**, 259 (1989).
[48] G.W. Lemire, G.A. Bishea, S.A. Heidecke, and M.D. Morse, J. Chem. Phys. **92**, 121 (1990).
[49] K. Raghavachari, J. Chem. Phys. **84**, 5672 (1986); K. Raghavachari and C.M. Rohlfing, *ibid.* **89**, 2219 (1988); P. Ballone, W. Andreoni, R. Car, and M. Parrinello, Phys. Rev. Lett. **60**, 271 (1988); W. Andreoni and G. Pastore, Phys. Rev. B **41**, 10 243 (1990); Z.Y. Lu, C.Z. Wang, and K.M. Ho, *ibid.* **61**, 2329 (2000).
[50] W. Andreoni, Phys. Rev. B **45**, 4203 (1992); Z. Phys. D: At., Mol. Clusters **19**, 31 (1991).
[51] G. Onida and W. Andreoni, Chem. Phys. Lett. **79**, 1770 (1997).
[52] M. Rohlfing and S.G. Louie, Phys. Rev. Lett. **80**, 3320 (1998).
[53] S. Öğüt, J.R. Chelikowsky, and S.G. Louie, Phys. Rev. Lett. **79**, 1770 (1997).
[54] I. Vasiliev, S. Öğüt, and J.R. Chelikowsky, Phys. Rev. Lett. **78**, 4805 (1997).
[55] J. Berkowitz, *Photoabsorption, Photoionization, and Photoelectron Spectroscopy* (Academic, New York, 1979).
[56] G.W. Lemire, G.A. Bishea, S.A. Heidecke, and M.D. Morse, J. Chem. Phys. **92**, 121 (1990).
[57] P. Y. Yu, M. Cardona, *Fundamentals of Semiconductors*, 1st ed. (Springer-Verlag, Berlin 1996).
[58] L.T. Canham, Appl. Phys. Lett. **57**, 1046 (1990); D.J. Lockwood, Solid State Commun. **92**, 101 (1994), and references therein.
[59] U. Itoh, Y. Toyoshima, H. Onuki, N. Washida, and T. Ibuki, J. Chem. Phys. **85**, 4867 (1986).
[60] S. Furukawa and T. Miyasato, Phys. Rev. B **38**, 5726 (1988); D.J. Lockwood, A. Wang, and B. Bryskiewicz, Solid State Commun. **89**, 587 (1994).
[61] M.V. Wolkin, J. Jorne, P.M. Fauchet, G. Allan, and C. Delerue, Phys. Rev. Lett. **82**, 197 (1999).
[62] T. Takagahara and K. Takeda, Phys. Rev. B **46**, 15 578 (1992).
[63] N.A. Hill and K.B. Whaley, Phys. Rev. Lett. **75**, 1130 (1995); **76**, 3039 (1996); C. Delerue, M. Lannoo, and G. Allan, *ibid.* **76**, 3038 (1996).
[64] C. Delerue, G. Allan, and M. Lannoo, Phys. Rev. B **48**, 11 024 (1993).
[65] L.W. Wang and A. Zunger, J. Phys. Chem. **98**, 2158 (1994); J. Chem. Phys. **100**, 2394 (1994).
[66] B. Delley and E.F. Steigmeier, Phys. Rev. B **47**, 1397 (1993).
[67] R.J. Baierle, M.J. Caldas, E. Molinari, and S. Ossicini, Solid State Commun. **102**, 545 (1997).
[68] A. Franceschetti, L.W. Wang, and A. Zunger, Phys. Rev. Lett. **83**, 1269 (1999); S. Öğüt, J.R. Chelikowsky, and S.G. Louie, *ibid.* **83**, 1270 (1999).
[69] R.W. Godby and I.D. White, Phys. Rev. Lett. **80**, 3161 (1998); S. Öğüt, J.R. Chelikowsky, and S.G. Louie, *ibid.* **80**, 3162 (1998).
[70] F. Kootstra, P.L. de Boeij, and J.G. Snijders, Phys. Rev. B **62**, 7071 (2000).